# Fast evaluation of the influence of simulated Acid Mine Drainage (AMD) on plant germination and growth using optical interferometric techniques

(光学的干渉法を用いた模擬酸性鉱山廃水(AMD)の種子の発芽および成長に対する影響の迅速な評価法)

Saitama University，Graduate School of Science and Engineering, Optical Sensing Laboratory (Doctoral Porgram)

Supervisor: Prof. Kadono Hirofumi

LI DANYANG

19DE068

SAITAMA UNIVERSITY

Doctoral Thesis

# Fast evaluation of the influence of simulated Acid Mine Drainage (AMD) on plant germination and growth using optical interferometric techniques

# 光学的干渉法を用いた模擬酸性鉱山廃水(AMD)の種子の発芽および成長に対する影響の迅速な評価法


Submitted by:

LI DANYANG

ID: 19DE068

Supervisor:

Prof. Kadono Hirofumi


2022

# Content

# List of Figures and Tables

## Figures

# Tables

# Acknowledgement

My PhD study life at Saitama University Optical Sensing Lab started in the fall of 2019. Although Covid-19 made my campus life special, I still received a lot of growth and emotions.

First of all, I would like to show my respect to my supervisor, Professor Kadono Hirofumi. I am thankful that he accepted me as his PhD student. I also would like to thank him for his guidance and support of my research, which has allowed me to continue to learn and improve. Your guidance and support for my research and your meticulous and conscientious qualities means a lot to me. I also would like to express my gratitude to Prof. Uma Maheswari Rajagopalan. She has helped me a lot in research and essay writing. I have learned a lot because of her patience and extensive writing experience.

I am deeply grateful for the academic guidance, comments, and suggestions given by committee members Prof. Kawai Yamada Maki, Prof. Fujino Takeshi, and Prof. O Seiyo. I would like to thank to Grant-in Aid for Japanese Society for the Promotion of Science of the Japanese Government and Ministry of Education, Culture, Sports, Science and Technology (Monbukagakusho) for providing financial support which enabled me to study in Saitama University. Thanks to the support and encouragement from my lab mates, members of the Environmental Science and Engineering Department at Saitama University, my family and my friends.

I really appreciate all the people who gave me support and help. This dissertation is impossible to complete without them. All my achievements come from their dedication.

# Abstract

Acid Mine Drainage (AMD) is one of the world's worst wastewater pollutions, and it causes a massive threat to crop. In this study, as a way to speedily monitor the effects of AMD on crops and non-destructively, we have proposed a technique named biospeckle Optical Coherence Tomography (bOCT) to evaluate biological activities of seed under the exposure of AMD, and bOCT was applied for kaiware daikon, soybean and rice after exposing to 40 ml/L and 80 ml/L simulated AMD for few hours and compared the results with conventional physical such as root and shoot lengths and physiological parameters such as enzymes. Comparison revealed that the effects due to the AMD could be seen within several hours by bOCT with a decrease in a parameter called bisopeckle contrast which reflects the internal activity of the seeds in comparison to the physical (shoot and root lengths) and physiological parameters such as seed vigor, antioxidative system, iron concentration that appear only after 7 to 10 days. Despite the fast measurement time bOCT, the results agree with conventional indicators with both showing the same tendency. Further, another optical interferometric technique, statistical interference technique (SIT), was used to monitor the nanoscale intrinsic fluctuations (NIF) of rice leaves exposed to simulated AMD. SIT proved to be reliable and sensitive to changes in the environment, making NIF a measure of plant health. Because of the non-invasive and sensitive nature of bOCT and SIT, we expect that biospeckle contrast and NIF have the potential to become valuable parameters in agriculture.

**Keywords**: Crop, Simulated acid mine drainage, Sustainable agriculture, Biospekle, Optical coherence tomography, Statistical interference technique

# Chapter 1 Introduction

## 1.1 Cause and risks of acid mine drainage (AMD)

Mineral resources are an indispensable primary raw material for social and economic development. However, mining inevitably causes damage to the environment and brings many adverse effects on the ecological environment and human health (Simate and Ndlovu, 2014). In mining mineral resources such as coal and metals, a large amount of mine wastewater is generated due to the oxidation of sulfide minerals contained in the minerals (Akcil and Koldas, 2006). Such mine wastewater has the characteristics of low pH (2-3), high level of Fe ions, and high $SO4^{2-}$, so it is called acid mine drainage (AMD) (Dong et al., 2018). The photo of AMD-polluted river that is brown color because it contains large amount of iron (Figure 1). The associated sulfide minerals in the ore are often weathered and leached to form acid mine drainage in coal or metal mines during mining and tailings stockpiling (Akcil and Koldas, 2006). It is important to note that AMD is not only generated during coal mining, but most metal mines are primary sulfide deposits. metal mines are mostly primary sulfide deposits, which can also be generated during mining activities or tailings stockpiles due to the biological oxidation of associated sulfide minerals AMD. AMD is a special kind of acid mine drainage, which cannot be directly recycled and is often discharged into the ecosystems of rivers, lakes and soils near the mines. The environmental pollution problem caused by AMD has become a hot issue in environmental science and soil science. The environmental pollution problem caused by AMD has become a hot issue in the field of environmental science and soil science and has received attention from researchers all over the world.

Furthermore, AMD discharged into rivers will cause the pH of the water body to decrease rapidly, leading to the death of aquatic organisms and weakening the self-purification ability of the water body (Chamorro et al., 2018; Mapanda et al., 2007). The infiltration of AMD into the soil could cause soil acidification, resulting in vegetation wither, causing even death. When AMD is discharged into a water body, it often changes the pH value of the water body, which inhibits or prevents the growth of bacteria and

microorganisms in the water body and affects the self-purification of the water body. When AMD enters the farm system with irrigation water, it can destroy the agglomerate structure of the soil, causing the land to become caked and the crops to die. In AMD-contaminated rice soils the maximum concentration of adsorbed sulfate was found in the 20-30 cm soil layer, where large soil particles, rich in amorphous iron hydroxide and fine clay enhanced the $SO4^{2-}$ adsorption (Wang et al., 2018).

AMD is a strong threat to the yield and quality of crops. Moreover, according to the UN Food and Agriculture Organization, the number of hungry people in the world is increasing every year, by 2020, 2.37 billion people are in food crisis (Organization, 2020). Therefore, the effects of AMD on crops are of interest to many researchers. For example, Huang X. et al. conducted a risk assessment of rice irrigated with AMD (Huang et al., 2016), SC Ma et al. investigated the effect of AMD on physiological characteristics and yield of winter wheat (Mapanda et al., 2007), Liao et al. investigated the migration of heavy metals in crops affected by AMD (Liao et al., 2016), AE Garrido et al. investigated the effect of AMD on agricultural soils and potatoes (Garrido et al., 2009), Prasad et al. evaluated treatment technologies for using AMD in agriculture (Prasad et al., 2021).

Figure 1 A river polluted by acid mine drainage. (https://www.p2w.co/about/acid-mine-drainage-water-pollution/)

## 1.2 Purpose and significance of the study

Optical coherence tomography (OCT) is a non-invasive imaging interferometry method that maps 2D or 3D depth-resolved tomographic images of internal tissue structures with speed, quality and high spatial resolution (Nemeth et al., 2013). And this technology is mainly used in biomedical research such as ophthalmology (Yang et al., 2018). In recent years, there has been an increasing number of studies on the application of OCT to plant science. Such as quantification of plant morphology and leaf thickness (de Wit et al., 2020), investigation of fungal disease on wheat leaves (Rateria et al., 2019), assessment of apple bitter-rot progression (Wijesinghe et al., 2018), microstructural changes in leaves during senescence (Anna et al., 2019), non-invasive classification of rice seeds (Joshi et al., 2021), imaging of plant root growth (Larimer et al., 2020), and detection of mold-contaminated peanuts (Manhando et al., 2021). Furthermore, our group has developed biospeckle OCT (bOCT) and validated the potential of bOCT in visualizing the response of leaves under ozone exposure (Srimal et al., 2013; Srimal et al., 2015), the biological activity of pea seed germination (Lim et al., 2019), the rapid visualization of applied phytohormones on plant leaves (Rajagopalan et al., 2020) and the phenotype of seeds in different concentrations of zinc (De Silva et al., 2021b) and microplastics(De Silva et al., 2022). To further confirm the feasibility of bOCT for monitoring plant response to AMD, in the current work, we selected kaiware daikon, rice and soybean, the staple food crop, as the subject in the current study. A different response between kaiware daikon, rice and soybean was also expected. In addition, some traditional physiological indicators were selected to compare with bOCT results.

A commonly used invasive chemical method for analyzing seed vigor, the TTC (Triphenyl tetrazolium chloride) test, was also used. It is used here to differentiate between metabolically active and inactive seeds after AMD exposure (Lopez Del Egido et al., 2017). Environmental stress like AMD could induce oxidative stress by causing the excessive accumulation of ROS (reactive oxygen species) such as $H_2O_2$ (hydrogen peroxide) (Sies, 2014). SOD (superoxide dismutase) and CAT (catalase) are the antioxidant enzymes in the antioxidant system to remove H2O2 and maintain cell membrane stability (Gajewska and

Skłodowska, 2008). Excess ROS can lead to cell membrane damage, and MDA (malondialdehyde) content which is a standard indicator of the degree of lipid peroxidation (Mittler, 2002). In addition, Fe concentration, shoot length and root length of seedlings were also measured for comparison with bOCT results.

By using statistical interferometry technique (SIT), we are able to measure instantaneous sub-nanometer displacements with high sensitivity, high speed, and non-invasive optics. SIT applied to plant leaf elongation revealed nanometric intrinsic fluctuations (NIF) that are reliable and sensitive to variations in the environment making NIF a measure of the healthiness of the plants.

Therefore, in this study, we used the staple food crops kaiware daikon, soybean and rice as experimental subjects to monitor the response of the seeds to different concentrations of AMD by bOCT in a rapid and non-invasive way, and to compare with the conventional methods mentioned above. Further, we applied SIT, focusing on the effect of AMD on NIF of seedling leaves to monitor the plant response to AMD.

# Chapter 2 Fundamentals of the speckle and biospeckle

## 2.1 Biospeckle Optical Coherence Tomography (bOCT)

Biospeckle is a nondestructive method for the evaluation of living objects. It has been applied to medicine, agriculture and microbiology for monitoring processes related to the movement of material particles. Recently, this method is extensively used for evaluation of quality of agricultural crops. In the case of botanical materials, the sources of apparent biospeckle activity are the Brownian motions and biological processes such as cyclosis, growth, transport, etc. (Zdunek et al., 2014).

### 2.1.1 biospeckle

Biospeckle provides a convenient tool for contact-less testing and monitoring of some industrial and biological phenomena of practical interest. The information is usually obtained by using first- and second-order statistics (Briers, 2001). In Fresnel speckle, obtained by free propagation, a huge number of simultaneous samples of intensity representing virtually the same state are registered. This feature provides the possibility of an efficient use of statistics.

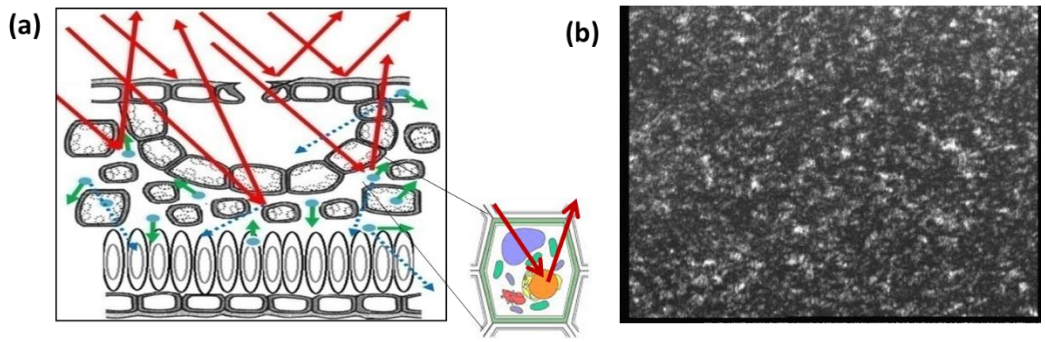


Figure 2 Causes of biospeckle pattern (a) and biospeckle pattern (b)

When laser light is shone on the plant, the scattered particles on the surface and inside of the plant scatter light and form speckle patterns (Figure 2a). The speckle shown in Figure 2 (b) is caused by the scattering of reflected light from biological tissues, so it is called biospeckle. This kind of biospeckle changes randomly according to the internal activities of plants, caused by movement in biological objects, such as cytoplasmic flow, organelle movement, cell growth, cell division, and biochemical reactions. When a plant is active, the biospeckle pattern will fluctuates over time. By combing this biospeckle and OCT, it's become possible to visualize the internal activity inside the plant. Therefore, we proposed bOCT.

### 2.1.2 bOCT experimental system

A schematic diagram of the spectral-domain optical coherence tomography (SD-OCT) is shown in Figure1. A superluminescent diode（SUPERLUM, SLD-137-HP3-DBUT-SM-PD, Ireland）with a central wavelength $\lambda_0$= 836.1 nm and a bandwidth $\Delta\lambda$ = of 55.2 nm providing a total outpower of 15.6mW was used as a light source. The light from the light source was first coupled to the input port of the circulator (AC Photonics, Inc. USA) and further divided into two beams by a 2 × 2 50/50 fiber coupler (TW850R5A2-2×2 Wideband Fiber Optic Coupler, 850±100nm, THORLABS, UK) illuminating the sample seed and the reference mirror, respectively. The reference arm consists of collimating lens L1, objective lens L4, and mirror M1, and the sample arm consists of lenses L2, L3 (LSM03-BB—Scan Lens, EFL = 36 mm, THORLABS, UK), and Galvano scanning

mirrors. Dispersion is compensated by a glass plate placed in front of the reference mirror followed by offline mathematical compensation following the collection of data. Light from L3 is reflected by mirror M2 to the seed. The power of the light incident on the seed in the sample arm was 2.6 mW that is below the irradiance damage threshold for seeds. The two-dimensional scanning mirror (Galvano mirror scanners) can scan laterally in the X and Y directions. The sensitivity was measured to be 96 dB at a depth of 0.24 mm. The sensitivity roll-off was around 7.94 dB/mm.

Each measurement is a 2048 (x) and 512 (z) raster scan over an area of 3.1 × 1.6 mm2 at an acquisition rate of 10 frames per second (fps). Hundred cross-sectional images were recorded. The fiber coupler recombined the backward scattered light from the seed and the reflected light from the reference mirror. This light was directed through a circulator to a spectrometer that consists of a collimator, lens L5, and a grating. The collimated light illuminated the grating to obtain spectral interference signal focused onto a line scan camera through lens L6. The spectra recorded by the spectrometer were mapped to K-space and then processed with a numerical dispersion compensation algorithm. To acquire the spectral interference signal, a line scan camera（L104k-2k, BASLER, Germany）with the number of pixels being 2048.

The depth-resolved reflectivity profile of the sample was obtained by Fourier transforming the spectral interference signal. The acquired OCT structure images were analyzed to calculate the contrast of the biospeckle. The depth resolution (axial resolution) of the system in free space was calculated as 6 μm using the following Equation (1), and the lateral resolution was calculated as 22 μm by Equation (2);

$$\Delta z = \frac{2\,ln\,{\lambda_0}^2}{\pi\, n\, \Delta\lambda}, \tag{1}$$

$$\Delta x = \frac{4\lambda_0}{\pi}\left[\frac{f}{d}\right], \tag{2}$$

where *f* is the focal length, *d* is the beam diameter, and *n* is the reflectivity index (n = 1.4).

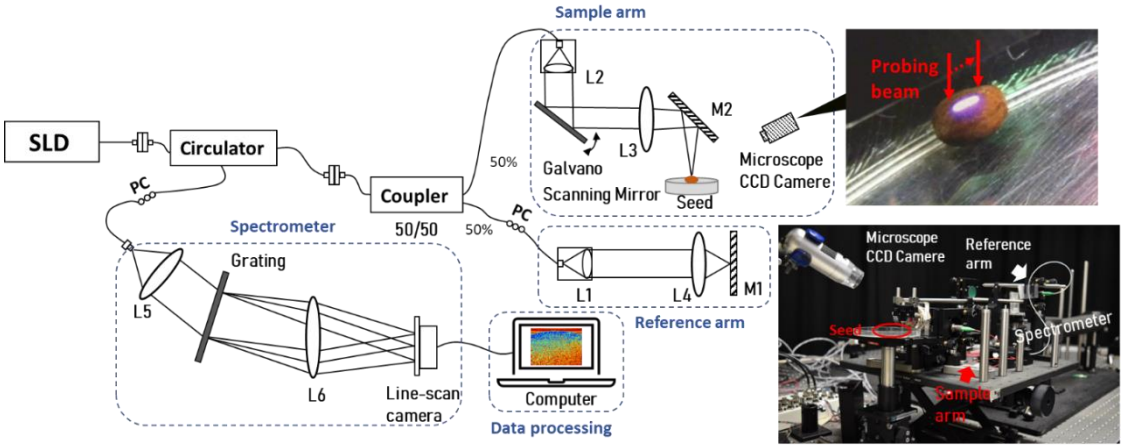


Figure 3 Schematic of Spectral Domain Optical Coherence Tomography (SLD: superluminescent diode, L1~L6: lenses, M1~M2: mirror, PC: polarization controller). Here, the microscope on the sample arm was used to adjust the seed orientation placed on a petri dish. The photograph shows a picture of the real system, with the encircled region showing the seed. The bright region on the seed indicates the scan line. A cover glass plate was used to partially compensate for the dispersion introduced by the objective lens in the sample arm. Dispersion was also compensated based on offline correction of the data after collection.

### 2.1.3 Biospeckle contrast

When a biological object is exposed to coherent light such as laser, the light is scattered on the object, and random interference between the scattered light produces a phenomenon called biospeckle (Aizu and Asakura, 1991). It is suggested that the dynamic behavior is resulting from the moving scatterers (Draijer et al., 2009). The intensity of the speckle pattern temporally remains constant for a static object. However, the dynamic changes of scattering centers caused by movement in biological objects, such as cytoplasmic flow, organelle movement, cell growth, cell division, and biochemical reactions, result in dynamic speckle patterns called as biospeckles. Reports on the use of biospeckles in monitoring the biological activities have been reported, for example monitoring apple fruit development prior to harvesting (Szymanska-Chargot et al., 2012), activity assessment of bacterial and parasitic organisms (Ramírez-Miquet et al., 2017), and identification of water activity change in carrots (Alves et al., 2013).

In the frames shown in Figure 4, because of biological activity, as shown in the Figure2, the intensity of one point would vary over time. The temporal variation is defined as the ratio of the standard deviation to the mean intensity of a single point calculated over a few seconds. It's called contrast. In this graph, the vertical axis is the intensity of the signal, and the horizontal axis is time. when the temporal variation is small, contrast is small and when the temporal variation is large, contrast is large. According to the contrast, we got biospeckle contrast images. temporal variation is higher in the red regions compared to blue regions (Figure 5a). Therefore, the changes in speckle contrast could be used to monitor the dynamics within the seed.

OCT images obtained contain speckles arising out of the movement of the scatterers within the seed tissue. Such resultant speckle pattern changes dynamically. The bOCT image is obtained by calculating the biospeckle contrast γ that is defined as the ratio of the standard deviation to the mean value of the biospeckle signal at each pixel along the temporal axis obtained from the successive OCT images with an acquisition interval of △ *t* and is given by,

$$\gamma\,(x,y) = \frac{1}{<I_{OCT}(x,y)>}\left[\frac{1}{N}\sum_{j=1}^{N}\{I_{OCT}(x,y;\,j) - < I_{OCT}(x,y) >\}^2\right]^{\frac{1}{2}} \qquad (3)$$

$$< I_{OCT}(x,y) >= \frac{1}{N}\sum_{j=1}^{N} I_{OCT}(x,y;j),$$

where *x, y* represents the pixel coordinates, *j* is the frame number, *N* indicates the total number of scans, *Ioct(x,y; j)* is the intensity at pixels (*x,y*) of a particular frame *j* and <*Ioct(x,y)*> is the mean of the images obtained over time.

The OCT structural images, acquired by averaging 100 OCT (x-z) scans, are shown in Figure 5 (b). In the region near to the seed coat and the slightly deeper region, a total of six specified rectangular localized regions, referred to as regions of interest (ROIs), were chosen. The selected ROIs are within 240 m of the seed surface, and the ROIs were chosen to be well within the system's sensitivity limitations. Equation (3) was used to calculate the biospeckle contrast of each ROI, and the average biospeckle contrast of each seed was calculated by averaging six ROIs (Figure 5b).

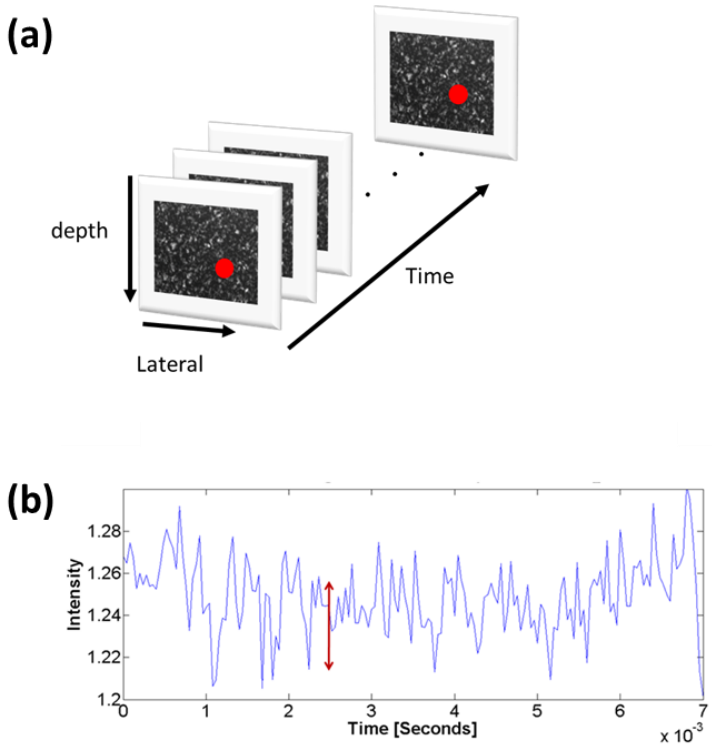


Figure 4 Time sequence speckle images for calculation of biospeckle OCT contrast (a) and reflected light intensity at one-point changes by time (b).

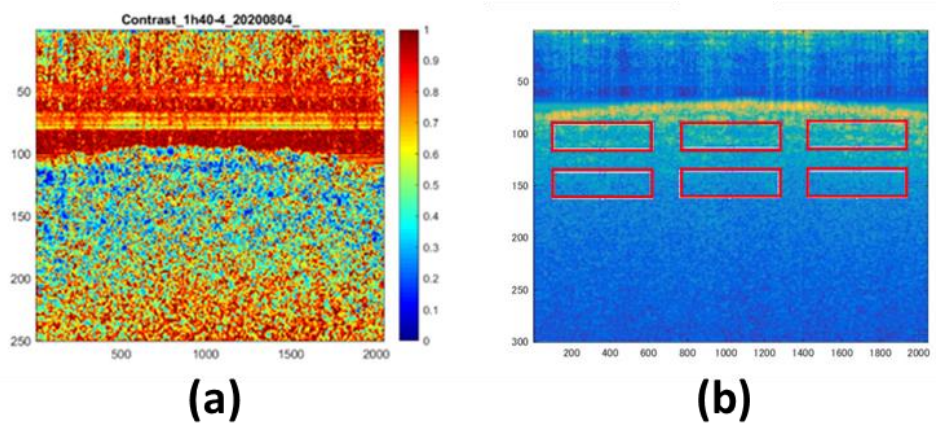


Figure 5 bOCT images (a) and OCT structural images (x-z) scans with six regions of interest (ROI) indicated by rectangles(b). Each rectangle corresponds to 512 x 25 pixels. The average contrast of the ROIs was used to calculate the average across six seed to give the grand average.

## 2.2 Statistical Interferometric Technique (SIT)

Speckles appear as a result of random interference of the scattered light by a rough surface object when it illuminates by a coherent light such as a laser beam and were considered as noise earlier. However, a theoretical interpretation of the laser speckle phenomenon has been developed, and this phenomenon was a recognized source of information on objects. There were a large number of applications proposed and developed using this phenomenon such as surface roughness measurements, speckle velocimetry, stellar speckles, and speckle interferometry. This technique has also been applied to biological objects such as blood flow measurements. This non-invasive technique using speckles has made them important making them no longer a random noise. It is important to understand the basics of the statistical properties of the speckles (Dainty, 1984) to understand the technique of statistical interferometric technique (SIT) that here we used.

Displacement is one of the most fundamental geometric parameters, and its accurate measurement is important for people to engage in various fields of research and promote scientific progress. On the one hand, compared with other mechanical quantities, displacement is easy to detect, and the detection accuracy is high, so the mechanical quantity of the object to be measured is often converted into displacement to detect, and the displacement sensor has therefore become the most basic sensor among mechanical quantity sensors. Among many micro-displacement measurement techniques, laser interferometry is widely used due to its unique advantages of traceability, non-contact measurement and high resolution.

The laser interferometric displacement measurement technique is based on the laser wavelength The laser interferometric displacement measurement technique is based on the laser wavelength, and the displacement is measured by the interference principle. Interferometry is a technique of waves, usually electromagnetic, are superimposed in order to extract information about the waves. Interferometry is an important investigative technique in the fields of astronomy, fiber optics, engineering metrology, optical metrology, oceanography, seismology, spectroscopy (and its applications to chemistry), quantum mechanics, nuclear and particle physics, plasma physics, remote sensing, biomolecular

interactions, surface profiling, microfluidics, mechanical stress/strain measurement, velocimetry, and optometry. Interferometers are widely used in science and industry to measure small displacements, changes in refraction index and surface irregularities. In analytical science, interferometers are used in continuous wave Fourier transform spectroscopy to analyze light containing features of absorption or emission associated with a substance or mixture. An astronomical interferometer consists of two or more separate telescopes that combine their signals, offering a resolution equivalent to that of a telescope of diameter equal to the largest separation between its individual elements.

Statistical interferometry technique (SIT) is a non-contact, real time monitoring optical interferometric technique. The principle of SIT is quite different from that of the conventional interferometric techniques (Hariharan, 2003).In a conventional interferometer, light reflected from an optically smooth reference mirror and that reflected light from the sample under observation interfere to give an interference pattern, and then the phase change is derived. In such a conventional interferometry, the sample must have an optically smooth surface for the phase analysis to be carried out. On the other hand, when an optically rough surface object is illuminated by a laser light, a fully developed speckle field is generated, and therefore the conventional interferometric technique is not applicable. Phase of such speckle field has a uniform probability density function (PDF) that takes a constant probability density of 1/2m over the phase range from $-\pi$ to $+\pi$ with the value of $1/2\pi$.

Such statistical properties of the speckle phase are very stable and independent of the surface properties. Those properties play the role of a standard in the object phase determination. In other words, SIT utilizes the complete randomness of the scattered light field as a reference in a statistical sense. This forms the foundation of SIT. SIT can be used to measure the displacement at sub-nanometer accuracy. We have been successful in the measurement of expansion of scattering objects and biological objects such as plants with SIT (Kobayashi and Kadono,2010; Rathnayake et al., 2007, 2008; Thilakarathne et al., 2014a,2014b). In those studies, temporal resolution of second could be achieved in the growth measurements of the plants with SIT.

# Chapter 3 Materials and Methods

## 3.1 Simulated AMD and Seeds

The main components in AMD are iron and sulfate. An amount of 0.744 g $FeSO4 \cdot 7H_2O$ dissolved in 250 ml distilled water was used to prepare the simulated AMD stock solution. It should be point out that the simulated AMD is different from the naturally occurring one in mine fields as simulated one does not contain any of the heavy metals such as Cu, Cr, Cd other than Fe. The stock solution was diluted with distilled water to get different concentrations of AMD. 40 ml AMD was volumized to 1 L with distilled water to get 40 ml/L AMD (pH = 2.7), and 80 ml AMD was volumized to 1 L with distilled water to get 80 ml/L AMD (pH = 3.0). The Fe concentrations of two AMD treatments were 24mg/L and 48mg/L, respectively and it is close to the normal pollution levels occurring at mine sites (Kiiskila et al., 2020). The simulated AMD is different from the naturally occurring one in mine fields as simulated one does not contain any of the heavy metals such as Cu, Cr, Cd other than Fe.

Here, we would like to point out that the bOCT method itself is new and we are not sure whether we would be able to visualize the effects of the application of AMD to rice. Fe and $SO_4^{2-}$ are major ions in natural AMD, Fe and SO42- are the main ions in natural AMD, and Table A 1 shows that the content of Fe is much higher than that of other metals (Matlock et al., 2002). Adding a trace of heavy elements to AMD would add difficulty in segregating the results on whether the effects are from the trace elements or the major elements (Fe and $SO_4^{2-}$). Moreover, the addition of trace metals would complicate the analysis of the results because of the different effects of different heavy metals. For example, Zn in suitable concentrations can be used as a nutrient to promote plant growth, while excess Zn can cause plant toxicity (De Silva et al., 2021). And if other heavy metals are added, the combined effect also needs to be considered. Therefore, in order to simplify the interpretation, we decided to use AMD that contained only Fe and sulfur and no trace of heavy metals.

During storage and before use, Kaiware daikon seeds (Tohoku seed company, Japan) , soybeans (Miyagi Prefecture Co., Ltd. Shosada, Japan) and the rice seeds (koshihikari) (Uken Co., Ltd. of Yamashina, Kyoto City, Japan) were kept at low temperatures and in dry conditions. The seeds were soaked in a 2.5% H2O2 solution for 15 minutes for surface sterilization and then washed three times with distilled water to remove residual disinfectant. Then carefully dry the water on the seed surface with a paper towel. After that, the seeds were placed in Petri dishes and same volume of simulated AMD was added so that the seeds were just immersed. Seeds were exposed to simulated AMD of different concentrations, while seeds exposed to distilled water were used as the control. All the seeds were kept in a growth chamber (SANYO Electric Co., Ltd., Osaka, Japan) under environmental conditions with a temperature of 29 ℃ for rice seeds, 26℃ for kaiware daikon and soybean seeds, a light intensity of 350 μmol $m^{-2}s^{-1}$, and a humidity of around 60%. Distilled water was used to replenish water loss from evaporation and transpiration every day. Six seeds or seedlings were used for each treatment.

## 3.2 bOCT method

Before the OCT measurement, the seeds were dried with paper towels to avoid moisture on the seeds from affecting the data. To ensure that OCT images of all the seeds are acquired from the same position, the seeds were needed to be adjusted and fixed in position and orientation before scanning. To achieve that, the cotyledon surface was set to be perpendicular to the laser beam, and the center of the cotyledon was irradiated. The embryonic axis was oriented such that it is parallel to the surface of the scan lens. We used a microscope CCD camera and an XYZ 3-Axis adjustable manual displacement platform to fine-tune the position of the seeds, ensuring that the light beam was incident on the center of the cotyledons of each rice seed. Six seeds used for each AMD treatment were scanned successively and replicated three times. A photo of the system with a typical seed used under the scan is shown in Figure 3.

## 3.3 Conventional method

### 3.3.1 Seed vigor

Seed viability was determined by the TTC method. The rice seeds were cut longitudinally then soaked in 0.1% TTC solution for 2 h. Intact whole soybean seeds and kaiware daikon seeds were soaked in 1% TTC solution for 3 h. The soaking was in dark conditions and the temperature was 30℃. The reduced TTC was extracted with ethyl acetate, and the absorbance values of the extracts at 485 nm were measured by spectrophotometer, and higher absorbance values represent stronger seed vigor. (Liu et al., 2014).

### 3.3.2 Antioxidant system response

On the determination of SOD, CAT and H2O2, each sample was weighed 0.2 g, placed in an ice mortar with a small amount of quartz sand and 2 ml of phosphate buffer (pH = 7.4), and ground into homogenate. The homogenate was poured into a centrifuge tube and centrifuged at 4°C at 15,000g for 15 minutes. The supernatant obtained after centrifugation is the enzyme extract, which was stored in a refrigerator at 4℃.

The enzyme activity of SOD and $H_2O_2$ content were assayed using assay kit (Wako Pure Chemical Industries, Ltd, Miyagi, Japan). The experimental procedures followed the instructions for the assay kit.

The determination of CAT activity was based on the method from Davies et al, and a decrease in absorbance of 0.1 in one minute is defined as one enzyme activity unit (U) (Davies and Swanson, 2001). Pipette 0.2 ml of enzyme extract into a test tube, then add 0.3 ml of Tris-HCl buffer and 0.5 ml of distilled water. The tubes were heated in a water bath at 25 ℃ for 3 min and 40 μL of 200 mmol/L $H_2O_2$ was added. The absorbance of the mixture solution at a wavelength of 240 nm was then immediately measured by spectrophotometer. Readings were taken every 30 seconds for a total of 3 minutes. CAT activity was calculated according to the following equation,

CAT activity ($U \cdot g^{-1}FW \cdot min^{-1}$) $= \triangle A_{240} \times Vt / 0.1 \times Vs \times t \times FW$

$\triangle A_{240}$ represents the average value of the change in absorbance over 1 min; *Vt* represents the total volume of enzyme solution (ml); *Vs* represents the volume of enzyme solution of measurement (ml); *FW* represents the fresh weight of the sample (g).

The MDA content was measured by thiobarbituric acid method (Ren et al., 2018). Weigh 0.3 g of fresh leaves, put them into a 4°C mortar, add a small amount of quartz sand and 2 ml of 0.05 mol/L phosphate buffer, and grind them into a homogenate. The homogenate was transferred to a test tube, and then 3 ml of 0.05 mol/L phosphate buffer was used to rinse the mortar in two portions, and the extracts were combined. Add 5 ml of 0.5% thiobarbituric acid solution to the extraction solution and shake well. Place the test tube in a boiling water bath and boil for 10 minutes. Immediately after 10 minutes, the tubes were removed and placed in a cold-water bath. After the tubes were cooled to room temperature, the supernatant was obtained by centrifugation at 3000g for 15 minutes. The absorbance of the solutions to be measured was measured at 532 nm, 600 nm and 450 nm using 0.5% thiobarbituric acid solution as blank. The MDA content was calculated by the following equation,

MDA（$\mu mol \cdot g^{-1}FW$） $= [6.452 \times （A_{532}-A_{600}） - 0.559 \times A_{450}] \times Vt / (Vs \times FW)$

Where *Vt* represents the total volume of the extract (ml); *Vs* represents the volume of the extract used for the determination (ml); *FW* represents the fresh weight (g).

3.3.3 Germination rate

A total of 30 kaiware daikon seeds were used per treatment. The number of germinated seeds in each treatment was counted every 12 hours followed by normalization by the total number to obtain the germination percentage in each period.

3.3.4 Water content

Seedlings were collected after seven days of growth in each treatment, washed with distilled water, dried with filter paper, and weighed on an electronic balance with an accuracy of 0.0001g to get fresh weight. The plants were then placed in an oven at 105 ℃

for 15 minutes to de-enzyming, and then the temperature was adjusted to 75 ℃ to dry to a constant weight. The dry weight of the plants was obtained by weighing with an electronic balance immediately after removing the plants from the oven. Water content of the plant is a common indicator of the water status of plant tissues. The water content affecting the growth condition of plants has a significant impact on the quality of fruits and vegetables (Hughes et al., 1970) and is defined by the following relation;

Water content = (Fresh Weight − Dry Weight)/ Fresh weight×100%.

3.3.5 Shoot and root lengths

The shoot and root lengths of seedlings were measured from photographs taken followed by analysis using the ImageJ software (Tajima and Kato, 2013).

3.3.6 Fe concentration

Seedling samples were dried and used for Fe concentration determination. The determination method was from Kos et al. and the measurement instrument was ICP-AES (Kos et al., 1996).

For the digestion of samples for analysis by ICP-AES, add 10 mL of 1:1 HNO3, mix the sample, and cover with a watch glass or vapor recovery device. Heat the sample to 95 ℃ ± 5℃ and reflux for 10 to 15 minutes without boiling. Allow the sample to cool, add 5 mL of concentrated HNO3, replace the cover, and reflux for 30 minutes. If brown fumes are generated, indicating oxidation of the sample by $HNO_3$, repeat this step (addition of 5 mL of conc. $HNO_3$) over and over until no brown fumes are given off by the sample indicating the complete reaction with $HNO_3$. Using a ribbed watch glass or vapor recovery system, either allow the solution to evaporate to approximately 5 mL without boiling or heat at 95 ℃ ± 5℃ without boiling for two hours. Always maintain a covering of solution over the bottom of the vessel.

After the step in last paragraph has been completed and the sample has cooled, add 2 mL of water and 3 mL of 30% $H_2O_2$. Cover the vessel with a watch glass or vapor recovery device and return the covered vessel to the heat source for warming and to start the peroxide

reaction. Care must be taken to ensure that losses do not occur due to excessively vigorous effervescence. Heat until effervescence subsides and cool the vessel.

Continue to add 30% $H_2O_2$ in 1mL aliquots with warming until the effervescence is minimal or until the general sample appearance is unchanged. Cover the sample with a ribbed watch glass or vapor recovery device and continue heating the acid-peroxide digestate until the volume has been reduced to approximately 5 mL or heat at 95 ℃ ± 5℃ without boiling for two hours. Always maintain a covering of solution over the bottom of the vessel.

For the analysis of samples for ICP-AES, add 10 mL conc. HCl to the sample digest cover with a watch glass or vapor recovery device. Place the sample on/in the heating source and reflux at 95 ℃ ± 5℃ for 15 minutes. Filter the digestate through Whatman No. 41 filter paper (or equivalent) and collect filtrate in a 100 mL volumetric flask. Make to volume and analyze by ICP-AES.

Inductively coupled plasma mass spectrometry (ICP) is a mass spectrometry method that uses an inductively coupled plasma to ionize the sample. It atomizes the sample and produces atoms and small polyatomic ions, which are then detected. It is known and used for its ability to detect metals and several non-metals in liquid samples at very low concentrations. It can detect different isotopes of the same element, which makes it a versatile tool for isotope labeling. Plasma is the ionization source for ICP, while positively charged ions are the mass analyzer for mass spectrometry. Generally, argon is used to generate plasma at high frequencies (30 MHz) with energies between 1000 and 2000 W, since most elements in the periodic table are excited and ionized in the plasma temperature range of 6000-10,000 K. The torch is made of quartz and consists of three concentric tubes through which the argon gas flows. When a sample is introduced into the plasma, it goes through desolation, vaporization, atomization, and ionization before entering the mass analyzer (Thomas, 2002). How ICP works: The sample, which must usually be in liquid form, is pumped at a rate of 1 ml/min, usually with a peristaltic pump, into an atomizer where it is converted into fine aerosols with argon gas at a rate of about 1 l/min. The fine droplets of aerosol make up only 1-2% of the sample and are separated from the larger

droplets by a spray chamber. The fine aerosol then exits the outlet tube of the spray chamber and is delivered to the plasma torch via a sample injector.

## 3.4 SIT method

A schematic of the experimental system of a statistical interferometer for measuring in-plane expansion of a leaf is shown in Figure 6 (a) with an inset photograph showing leaf attached to a holder and a photograph of the SIT system in Figure 6 (b) on an optical bench. As a light source, a He–Ne laser of wavelength 632.8 nm (GLG 5400, NEC Corporation, Japan) was used. At first, light was passed through a neutral density filter (F71N-2 Suruga Seiki, Japan) to adjust the level of the light intensity on the leaf surface. Next, using a specially designed prism, P1, the laser beam was divided into two beams. A right angle prism, P2, mounted on a piezoelectric transducer (PZT) stage (E-620, Physik instrument, Germany) was employed to introduce path difference between the two illuminating beams. Plant leaf was mounted with a custom-made holder to measure the in-plane elongation or shrinkage of the surface of the leaf between the two probing points of the laser beam. It should be pointed out that base and the tip of the leaf were gently placed within the clamping gaps of the holder. To avoid damage to the leaf, cotton was used to cover the holder. The measurement position was around 2.2 cm from either side of the clamping positions. The leaf elongation was in the order of a few tens of micrometer within 24 h and this in comparison to the clamping positions is around 1,000 times smaller and so the clamp is expected to have no influence on the measurement.

When leaf surface is illuminated by laser light, a fully developed speckle pattern is generated (refer to Figure 3, De Silva et al. 2016) due to a random interference of the scattered light from the rough leaf surface. A charge-coupled device (CCD) (XC-75, Sony Corp., Japan, 768×494 pixel) was used to acquire the speckle interference pattern between the speckle fields generated from two probing beams. Generally, with leaf, a living biological tissue, two different kinds of speckle patterns arise from the scattered light. One is generated from the leaf surface and, the other from the laser light that penetrates deeper

into the leaf. In SIT measurements, the speckles that are from the surface has to be used in measurements while suppressing those from within the leaf.

The speckles originating from within the leaf are due to the moving scatterers such as organelles within the leaf and are also known as biospeckles (Goodman 2007), and the intensity of such speckles vary with time. Such fluctuation in intensity of the biospeckles would result in degradation of SIT measurements, and thus the biospeckle has to be reduced. To reduce this biospeckle variation, the laser beam that is penetrating within the leaf has to be reduced. In order to reduce the penetration, illuminating area was covered with wheat flour. In real time measurement, contribution of laser biospeckle generation was confirmed to be less than 0.04% of the incident probing beams (Thilakarathne et al. 2014b).

The Phase difference was measured by using this equation,

$$\Delta\varphi = \frac{2\pi}{\lambda}\,\Delta L\,\sin\theta$$

Where $\lambda$ is wavelength of light, $\Delta L$ is in-plane elongation of leaf and $\theta$ is the angle between the illumination and observation direction.

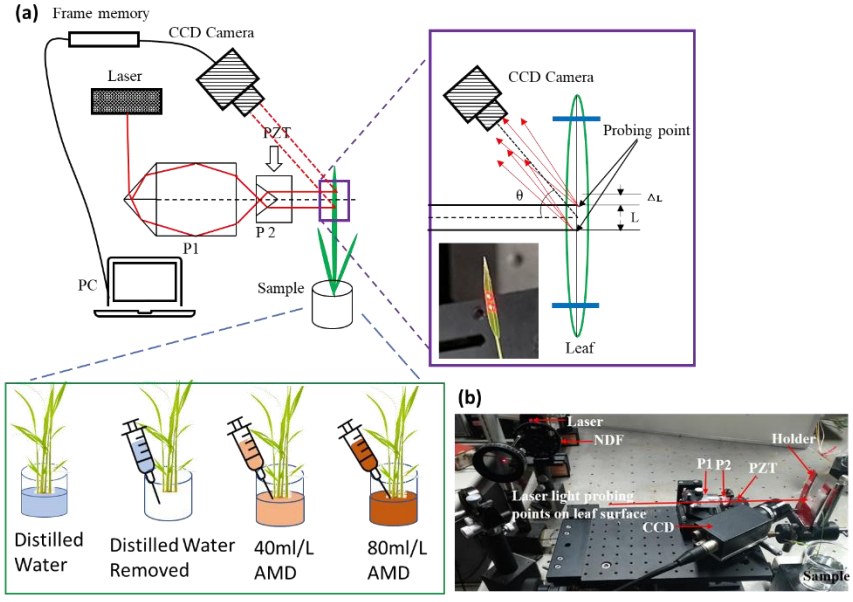


Figure 6 schematic of the SIT system used in this study with an inset photograph of leaf attachment with holder (a), a photograph of the SIT system. Plant leaf is stably and gently placed in the holder (b). The illumination point of laser light was about 2.5–3 cm apart

from leaf apex, and the distance between two probing laser beams was 3 mm. NDF, neutral density filter; P1 and P2, prism; PZT, piezoelectric transducer; CCD, charge coupled device.

Rice seeds were soaked in 2.5% hydrogen peroxide for 15 minutes to sterilize the seed surface, and then the seeds were rinsed three times with distilled water for the purpose of removing residual hydrogen peroxide from the seed surface. The sterilized seeds were placed in petri dishes lined with germination paper and the seeds were submerged with distilled water. The petri dishes were kept in a growth chamber (SANYO Electric Co., Ltd, Japan), and the growth conditions were maintained at an air temperature of 29 ◦C, a light intensity around 350 μmol $m^{-2}$ $s^{-1}$/0 μmol $m^{-2}$ $s^{-1}$ following a 12 h/12 h cycle, and relative humidity around 60%. Distilled water was replenished daily to ensure normal growth of the rice. The rice seeds grew into seedlings after one week and were used for SIT experiments.

The first new leaves of rice seedlings with flour on the surface were fixed in a special homemade holder and then monitored for 3 hours by SIT. The roots of seedlings were in distilled water for the first 1.5 hours and in mock AMD solution for the second 1.5 hours. The change of solutions was done by injector.

## 3.5 Data Analysis

Matlab 2016 was used to calculate the biospeckle contrast images from OCT temporal images and analysis of the NIF obtained by SIT. The significance between treatments was tested using the LSD (Least Significant Difference) test (Williams and Abdi, 2010) of IBM SPSS Statistics 26 software ($p<0.05$).

# Chapter 4 Monitoring the responses of different seeds to AMD by bOCT

## 4.1 bOCT Results and Discussion

### 4.1.1 Monitoring kaiware daikon seeds by bOCT

OCT images of the Kaiware daikon seeds exposed under different AMD concentrations of control, 40ml/L, and 80ml/L AMD after an exposure of 1 hour to AMD are shown in Figure. 7 (top row) with logarithmic intensity scale. Reflectivity signals of the OCT images can visualize the internal laminar structure of the seed. Bright regions correspond to stronger OCT reflectivity signal, while dark regions correspond to reduced reflectivity. At the very top, the seed coat, the epidermis, can be seen with greater reflectivity. There is also noise related to strong scattering due to the inhomogeneous nature of the structures within the measurement volume determined by the coherence of the source. The scattered light interferes to produce a granular pattern called biospeckle that changes with time due to the activity within the seed tissue.

From a series of OCT frames acquired in a few seconds, the bOCT images were calculated across the acquisition period under each of the conditions, namely, control, 40ml/L AMD, and 80ml/L AMD, and are respectively shown in Figure 7 (bottom row). As can be seen in Figure 7 (top row), there are no differences seen in the structural images with the change of AMD concentrations. On the other hand, comparing the biospeckle images obtained under different conditions, a clear difference could be seen. In the bOCT images, red regions correspond to higher temporal variation while blue regions correspond to lower temporal fluctuation. There are more red regions in the bOCT images for seeds exposed to AMD than those of control. Moreover, the bOCT image of seed in 80ml/L AMD has more red parts than those exposed to 40ml/L AMD.

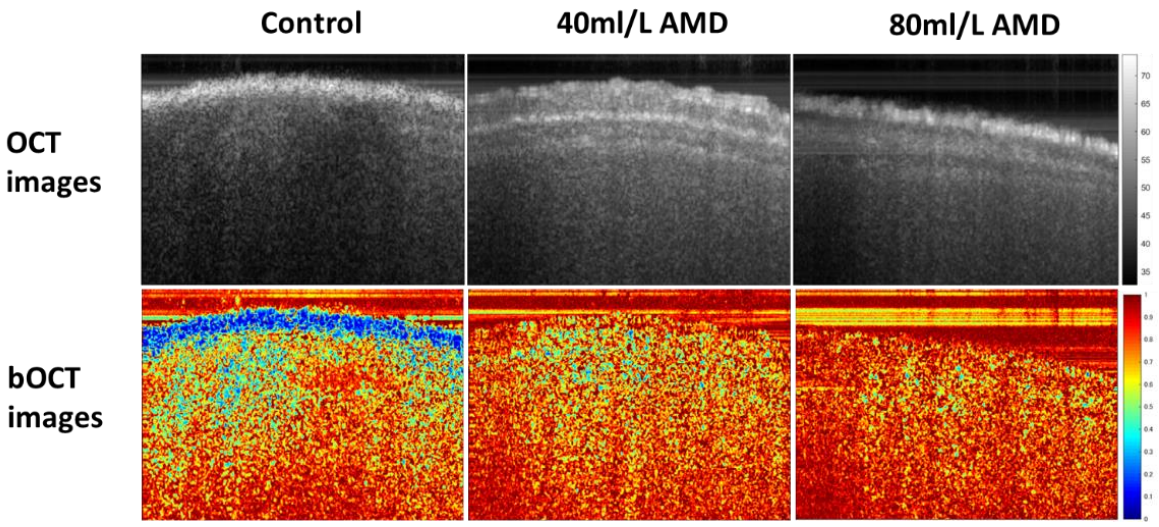


Figure 7 Cross sections of OCT structural (top row) and bOCT (bottom row) images after just an hour of AMD exposure for or control, 40ml/L AMD and 80 ml/L AMD.

The bOCT images can be used to know the trend of changes between different treatments, and further quantitative analysis of the bOCT images can be performed to analyze the significant differences between different treatments. Figure S1 shows the OCT structure images obtained by averaging 100 OCT (x-z) scans. A total of six specific rectangular localized regions, namely the regions of interest (ROIs), were selected in the region close to the seed coat and from the slightly deeper region. The depth of the selected ROIs is within 240μm below seed surface; the choice of ROIs is well within the sensitivity limits of the system. The biospeckle contrast of each ROI was obtained by Eq. (3) in the method section, and six ROIs were averaged to obtain the average value of the biospeckle contrast of each seed (Supplementary figure). Next, six seeds were measured for each treatment. A grand average of the biospeckle contrast calculated from six seeds was calculated and is shown in Figure 8.

In the figure, the biospeckle contrast values of the seeds under different treatments showed significant differences: 80ml/L > 40ml/L > control. The results indicate that the activity of the seeds was significantly different from that of the control after 1 hour of AMD treatment, and the contrast of the seeds under 80ml/L AMD treatment was significantly higher than that under 40ml/L AMD. Next, we compared the contrast with the germination rate.

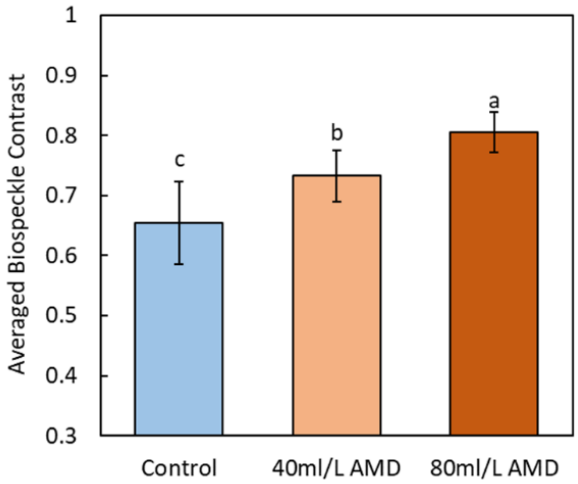


Figure 8 Averaged biospeckle contrast values of 6 seeds under each treatment after an exposure for one hour (Different letters represent statistical differences between treatments, The error bar represents standard deviation, Fisher-LSD multiple comparison, $p < 0.05$ level, Number N=6).

The germination could be affected by many factors such as humidity, light levels. The structure of seed changes dynamically during germination, and this is dependent on the pH of the medium used for germination. Environmental stress or stimulation, such as the presence of AMD, can affect the metabolic rate, organelle morphology, and locomotion rate of seeds and plants (Wang et al., 2020b). AMD has the effect of changing the pH of the medium and thus becomes an environmental stress introducing physiological changes during seed germination. We expect such physiological changes would lead to changes in scatterers or organelles within the seed. This, in turn, would lead to changes in the intensity of the random interference pattern or a change in biospeckles. Thus, the changes observed under different AMD treatments could be hypothesized to be related to the biological activity of the seed. Moreover, depending on different time points, namely one hour and also at 48 hours, the effects due to AMD could be different.

It is well known that seed vigor is proportional to germination speed (De Silva et al., 2021a; Marcos, 2015). To test the hypothesis, we monitored the percentage of germination of seeds within 48 hours (Figure9). As shown in Figure 9, the germination percentage of seeds treated with 40ml/L and 80ml/L AMD was higher than that of the control within 36 hours, while the germination rate of seeds treated with 80ml/L AMD was the highest.

However, at 48 hours, the germination percentage of all the treated seeds reached 100%. The results showed that AMD could improve the germination speed of seeds, and the germination speed of seeds was proportional to the seed vigor. The results may indicate that the seed vigor within 48 hours was 80ml/L AMD＞40ml/L AMD ＞Control. These results were consistent with the biospeckle contrast comparison trend obtained just 1 hour later, and this confirmed the hypothesis that bOCT could reveal vigor speedily.

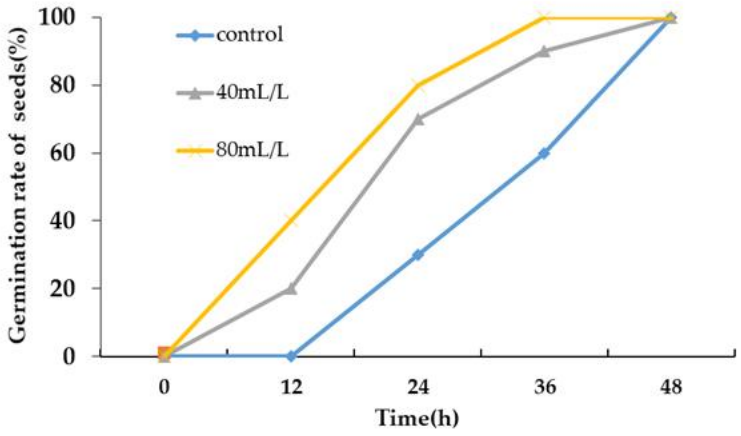


Figure 9 Percentage of seed germination under different treatments.

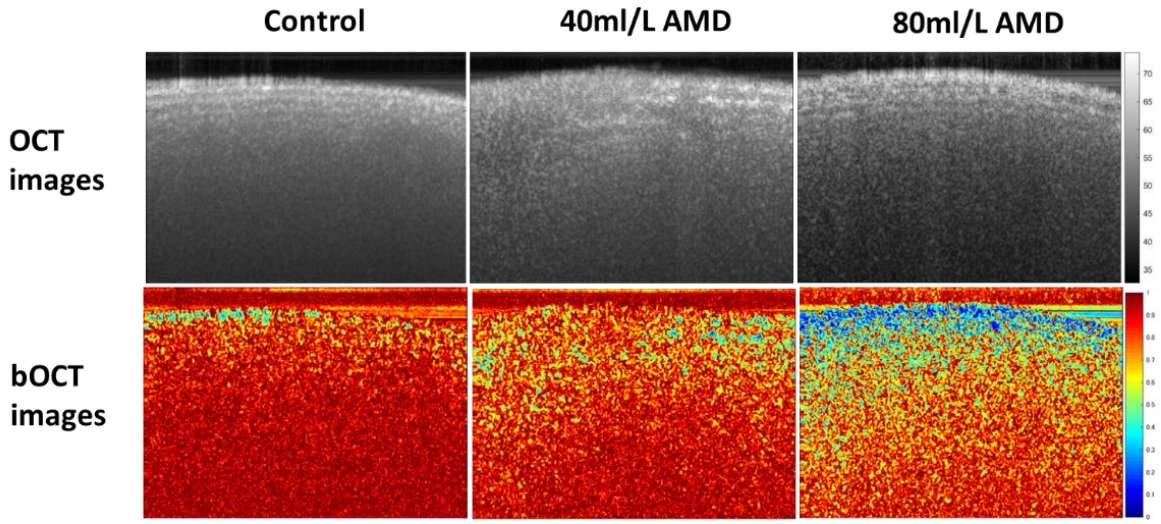


Figure 10 Cross sections of OCT structural (top row) and bOCT (bottom row) images of Kaiware daikon seeds after 48 hour of AMD exposure for 0 ml/L or control, 40ml/L, and 80 ml/L.

The percentages of seeds germinated at 48 hours under different treatments were the same (Figure10), and there was no noticeable difference in appearance. Therefore, we decided to investigate if there are differences in the internal activity of seeds at 48 hours. The bOCT method was used to monitor the seeds under different treatments, which did not damage the germinated seeds and was beneficial to observe the subsequent growth of seeds.

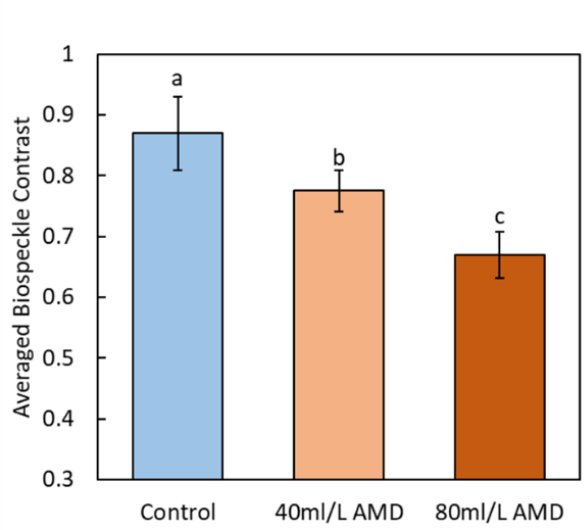


Figure 11 Averaged biospeckle contrast value of kaiware daikon seeds under different treatments after 48 hours exposure. (Different letters represent statistical differences between treatments, The error bar represents standard deviation, Fisher-LSD multiple comparison, $p < 0.05$ level, Number N=6).

OCT images of the Kaiware daikon seeds exposed under different AMD concentrations of control, 40ml/L, and 80ml/L AMD after an exposure of 48 hours to AMD are shown in Fig 10 (top row). There were no significant differences seen in the structural images with the change of treatment.

The bOCT images of seeds exposed to different treatments for 48 hours are shown respectively in Figs 10 (bottom row). A clear difference could be seen due to different AMD concentrations. The temporal variation is higher in the red regions compared to the blue regions. The blue part was more in the AMD treatment than in the control, indicating that the temporal variations in the AMD treatments were lower than that in the control after 48 hours. The temporal change in the 80 ml/L AMD treatment was lower than that in the 40 ml/L AMD treatment.

Figure 11 is obtained by calculating averaged biospeckle contrast of 6 seeds under each treatment. The results showed that there were significant differences between the treatments. The contrasts of seeds under AMD treatments were significantly lower than that of control, and the biospeckle contrast of seeds exposed to 80 ml/L AMD was significantly lower than that under 40 ml/L AMD (Figure11).

The current study investigates the application of biospeckle OCT to monitoring the dynamic changes during seed germination and that too under the presence of AMD. The structure of seed changes dynamically during germination. So, in practice, OCT, a technique that visualizes structures, should be capable of monitoring structural changes. However, because the structural changes are random generating random changes in OCT intensity, we proposed to use biospeckle OCT for investigating seed germination under AMD.

Further, the germination could be affected by many factors such as humidity, light levels, and environmental stress. AMD, one such environmental stress, can affect the metabolic rate, organelle morphology, and locomotion rate of seeds and plants (Wang et al., 2020b). During germination, the structure of seed changes dynamically, and this is dependent on the pH of the medium used for germination.

AMD has the effect of changing the pH of the medium and thus becomes environmental stress introducing physiological changes during seed germination. We expect such physiological changes would lead to changes in scatterers or organelles within the seed.

As possible scatterers, there are several internal microstructures such as mitochondria, Golgi bodies, and possibly chloroplasts within the seed. The movement of such structures from cell growth, cell division, cytoplasmic flow could contribute to the slow to rapid changes that would lead to changes in the intensity of the random interference patterns; in other words, changes in biospeckles observed in the bOCT images. Therefore, external environmental stress can affect those movements (Houston et al., 2016; Mangabeira et al., 2011; Srivastava et al., 2012), leading to the difference in bOCT images of the seeds treated with AMD at different concentrations.

Murata et al. (Murata et al., 2003) studied the effect of different pH (3.0-6.0) on germination and seedling growth of groundnut. They found that low pH did not affect seed germination but significantly reduced seedling survival and growth. The results on seedling growth are consistent with our findings. However, low pH AMD accelerated the germination of kaiware seeds in this study. There are two possible reasons as follows: Low pH accelerates the softening of the hard seed coat of kaiware, allowing water to enter the endosperm more quickly. The water enters and softens the seed coat, and oxygen penetrates more easily, enhancing the embryo's respiration and making it easy for the embryo to break through the seed coat (Taiz and Zeiger, 2002). In addition, other studies have shown that FeSO4 can promote seed germination (Khan et al., 2019; Moatter et al., 2020).

The elements Fe and S contained in AMD are essential elements for plants, but the results of bOCT at 48 hours and biomass after 7 days showed that the plants under AMD treatment were in poor condition. Islam A et al. (Islam et al., 1980) studied the effect of different pH nutrient solutions on ginger, cassava, maize, wheat, French beans, and tomatoes. The results showed that the damaging effects of low pH on the root system were observed in all species. At pH 3.3, roots of all species were shortened, thickened, relatively few in number, turned brown or dark gray in color, and the lateral root growth severely inhibited. The roots are an essential part of nutrient transport, and poor root growth will affect the growth of shoots. This is consistent with the findings of the present study that the negative effect of AMD on seedlings is higher levels of AMD or lower pH affecting macro growth. Our studies with bOCT also suggest low pH can have a significant effect on the earlier stages of germination, thus possibly shortening overall duration requirements for the case of kaiware daikon species.

### 4.1.2 Monitoring soybean seeds by bOCT

The dried soybean seeds used in this experiment were soaked in AMD for 6 hours to complete the water absorption and expansion then germination started after 48 hours. To determine whether AMD affected the internal activity of the seeds during this period, OCT images (Figure 12a) and bOCT images (Figure 12b) of soybean seeds exposed to different

concentrations of simulated AMD for 6 h and 48 h were obtained. OCT images showed the structure of the seed cross-section, which is static information, while bOCT images revealed the changes in biological activity inside the seed, which is dynamic information. From the OCT images (Figure 12a) we could not clearly distinguish the difference between the treatments either after 6 hours or 48 hours. Based on Equation (3), the bOCT images in Figure 12(b) were calculated from the corresponding OCT images (Figure 12a).

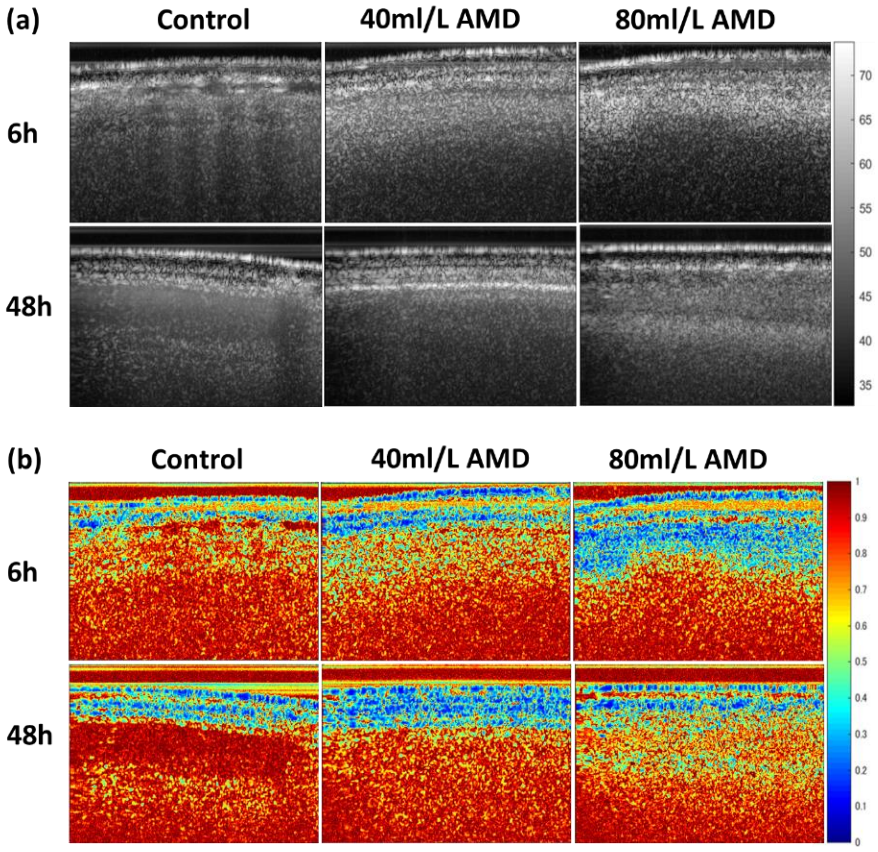


Figure 12 OCT images (a) and bOCT images (b) of soybean seed exposed in AMD for 6 and 48 hours.

A red region in the bOCT image corresponds to higher temporal fluctuations and a blue region to lower temporal fluctuations. There is greater activity or movement within the seed in the bOCT images with a higher red color density. A high blue color density, in contrast, indicates a lower level of biological activity or movement within the seed. Figure 12b (top row) showed more blue regions in the bOCT image of seeds treated with AMD for only 6 h compared to the control. Furthermore, there were more blue regions in the

bOCT images of the 80 ml/L AMD-treated seeds than in the bOCT images of the 40 ml/L AMD-treated seeds after 48 h, and both were clearly more than the control.

The bOCT images were further quantified and analyzed for significant differences between the treatments. The averaged biospeckle contrast for soybean seeds under different AMD treatments can be obtained by calculating the biospeckle contrast over specific local regions of interest (ROIs) in the bOCT image (Figure 13). In seeds exposed to 80 ml/L AMD treatment, the averaged biospeckle contrast was significantly lower than that in control seeds after 6 h. However, the difference between the averaged biospeckle contrast of the seeds in the low concentration AMD (40 ml/L) treatment and the control was not yet significant. The averaged biospeckle contrast of seeds under 40 ml/L AMD treatment showed significant decrease after 48 h compared to control. And the aver-aged biospeckle contrast of the seeds in the 80 ml/L AMD treatment was significantly lower than that in the 40 ml/L AMD treatment. The bOCT results indicated that the internal biological activity of soybean seeds was found to be inhibited by 80 ml/L AMD only after 6 h based and the inhibitory effect of 40 ml/L AMD on soybean seeds after 48 h was observed.

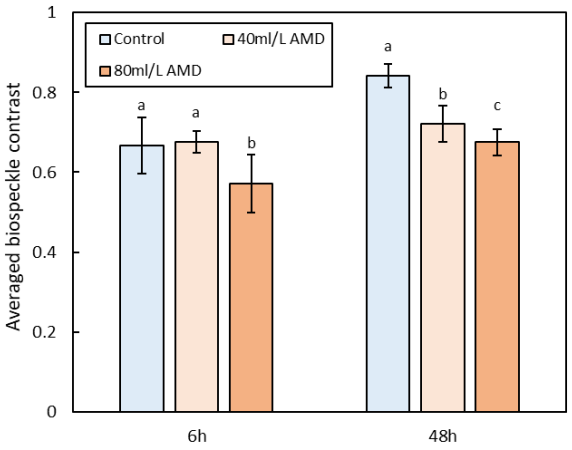


Figure 13 Averaged biospeckle contrast of seeds exposed in AMD for 6 and 48 hours. (Different letters, a b c, represent statistical differences between treatments; the error bar represents standard deviation; Fisher-LSD multiple comparison; $p < 0.05$ level; $N = 6$)

The higher the AMD concentration, the lower the internal activity of soybean seeds monitored by bOCT. The red color in the bOCT image represents high biospeckle contrast, high internal biological activity, while the blue color represents low biospeckle contrast, i.e. low internal biological activity. In contrast, OCT images do not reveal such difference

within the plant. Lim et al. demonstrated that the contrast of seeds inactivated by high temperature was much lower than that of seeds germinated at room temperature, suggesting that the biospeckle contrast measured by bOCT can quantify the biological activity of seeds during germination (Lim and Kadono, 2020). Changes in bOCT results before and after application of hormones were found to be statistically significant by Rajagopalan et al (Rajagopalan et al., 2020). Further, the effect of AMD on radish seed germination speed was found to be predicted by bOCT results in our previous study(Li et al., 2021). These studies from our group indicated that biospeckle contrast can capture the effect of environment on the internal biological activity of the plant.

Water is essential for the germination of seeds. In low pH solutions like AMD, the hard seed coat softens, allowing the seed to better absorb water and allowing the embryo to penetrate through the seed coat more easily. Seed respiration and organic matter conversion begin after water concentration. Soybean seeds mainly contain proteins, fats, which are gradually converted to glucose for germination and this process requires the joint participation of different organelles(Taiz et al., 2015). Organelles inside the plant such as mitochondria, chloroplasts and vesicles are possible scatterers and changes in the external environment can affect the movement of organelles(Perico and Sparkes, 2018; Wada and Suetsugu, 2004). These may account for the differences in bOCT results caused by different concentrations of AMD.

#### 4.1.3 Monitoring rice seeds by bOCT

OCT observations were performed for each seed sample at 24, 48 and 72 h after exposure to different AMD concentrations. The OCT intensity or reflectivity structural images in logarithmic scale are shown in Figure 14(a) for rice seed under different AMD concentrations after 24, 48 and 72 h. A laminar structure can be seen. Here, bright region indicates a strong OCT reflectance signal while a dark region corresponds to a weak reflectance signal. In either case, under exposure to AMD, the OCT images obtained under control, did not differ significantly from the seeds exposed to 40 ml/L AMD and 80 ml/L AMD.

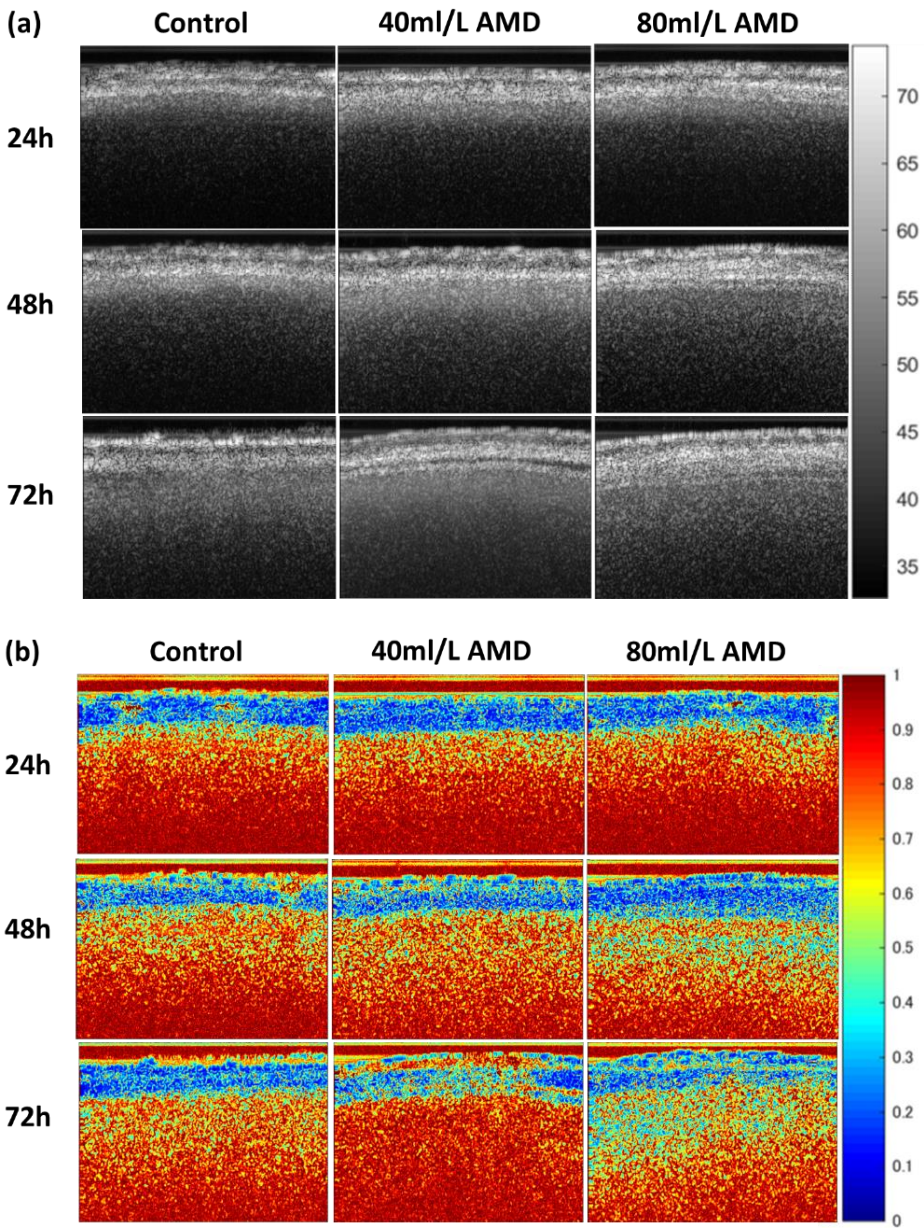


Figure 14 OCT images (a) and bOCT images (b) of rice seed exposed in AMD for 24, 48,72 hours.

On the other hand, in Figure 14(b) significant difference could begin to be seen in the bOCT results for rice under different AMD concentrations, exposed to AMD after 48 h. In the bOCT images, red regions correspond to higher temporal variations while blue regions correspond to lower temporal fluctuations. Comparing with the structural images, difference due to different treatments that were not visible in the OCT images could be clearly seen in the bOCT images. There are fewer red regions in the bOCT images for seeds

exposed to 80 ml/L AMD for 48h than those of the control and 40 ml/L AMD. Again, in the bOCT results of rice seeds exposed to AMD for 72 h, it can be observed that the rice seeds in 40 ml/L AMD have more red parts than control while the rice seeds in 80 ml/L AMD have more blue parts in the bOCT images

Seeds cannot germinate without water. low pH accelerates the softening of the hard seed coat, which accelerates the water concentration by the seed, and also makes it easy for the embryo to break through the seed coat. Respiration and organic matter conversion begin after the seeds have absorbed water. Starch, the main component of rice seeds, is gradually broken down into glucose for embryo growth. And This process requires the joint participation of different organelles. (Taiz et al., 2015). In addition, Khan et al. showed that $FeSO_4$ in proper concentrations would promote seed germination(Khan et al., 2019). The biospeckles observed in OCT images arise from the moving scatterers. As possible scatterers, there are several internal microstructures such as mitochondria, Golgi bodies, and possibly chloroplasts within the seed. The movement of these structures are possibly brought about by cell growth, cell division and cytoplasmic flow and such movements would change the biospeckles observed in the bOCT images. Environmental stresses such as AMD could affect plant metabolism, organelle movement and cell division (Wang et al., 2020a; Williamson, 1993). Therefore, the changes in seed structure and metabolic activity caused by different concentration of AMD may affect the intensity variation of the random interference pattern, which is the biospeckle variation that could be observed in the bOCT images. The bOCT images of rice seeds after 72 h in AMD revealed the different responses to different concentrations of AMD. Biological movements of rice seeds were more active in 40ml/L AMD. There are more red parts in the bOCT image of rice seeds in 40 ml/L of AMD, indicating that 40 ml/L AMD promoted metabolic activities during seed germination.

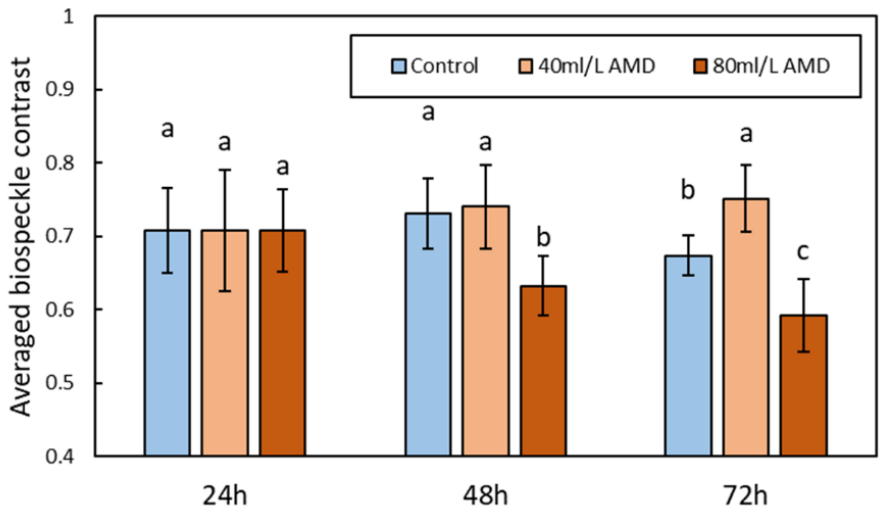


Figure 15 Averaged biospeckle contrast of rice seeds exposed in AMD for 24, 48, 72 hours. (Different letters, a b c, represent statistical differences between treatments; the error bar represents standard deviation; Fisher-LSD multiple comparison; $p < 0.05$ level; $N = 6$)

To analyze whether the changes in internal activity were significant, the bOCT images were quantified to obtain average biospeckle contrast. The comparison of average biospeckle contrast between all the treatments is shown in Figure 15. The average biospeckle contrast of rice seeds exposed in AMD for 24 hours did not show differences compared to the control. After 48 h, the average biospeckle contrast of rice seed in 80 ml/L AMD was significantly lower than that of the control and 40 ml/L AMD, and there was no significant difference between the control and 40 ml/L AMD. For the case of rice seeds after 72 hours exposure, the averaged biospeckle contrast in 40 ml/L AMD was 8.8% higher than that of control, while the averaged biospeckle contrast of rice seeds in 80 ml/L AMD was 9.6% lower than that of the control. We found that 40 ml/L AMD significantly promoted the biological activity of rice seeds.

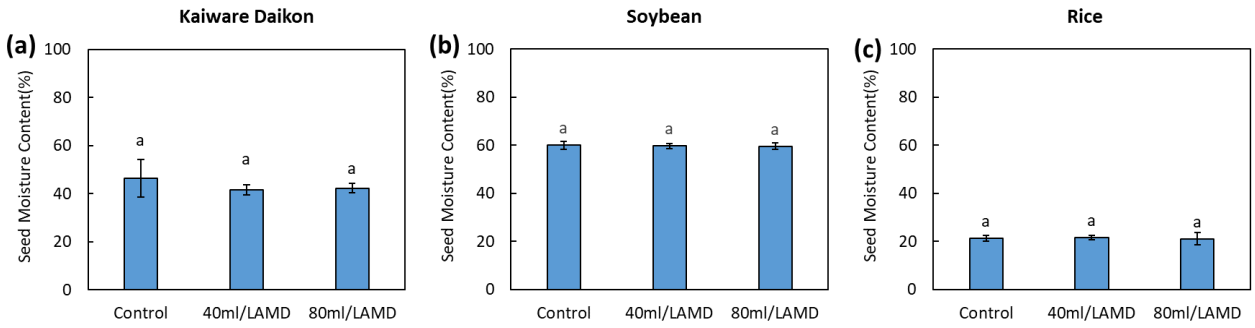


Figure 16 Seed moisture content of kaiware daikon seeds and soybean seeds exposed to AMD for 48 hours and rice seeds exposed to AMD for 72 hours.

Seed moisture content of kaiware daikon seeds and soybean seeds exposed to AMD for 48 hours and rice seeds exposed to AMD for 72 hours were determined (Figure 16). To demonstrate that kaiware daikon seeds, the source of significant differences in average biospeckle contrast between soybean seeds and rice seeds after 48 and 72 hours was not the seed water content. The results showed that while average biospeckle contrast showed significant differences, the differences in water content of the three seeds in the different treatments were not significant. This indicated that the difference in average biospeckle contrast between treatments was not due to the difference in seed moisture content.

## 4.2 Conventional Results and Discussion

### 4.2.1 TTC test

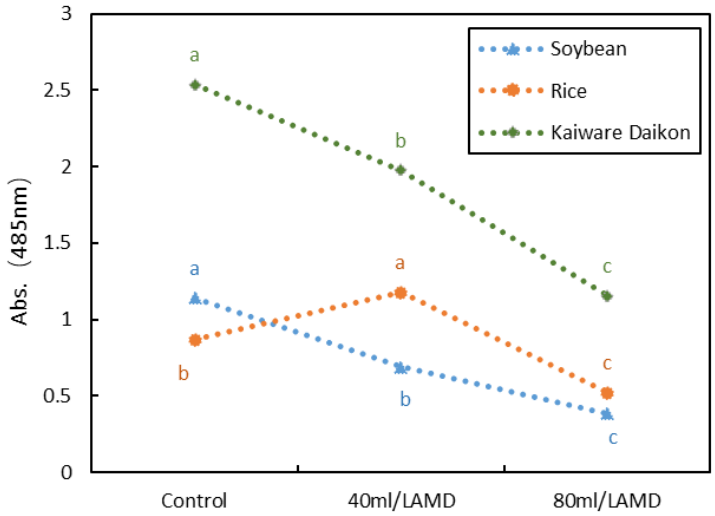


Figure 17 Seed Vigor of soybean seeds and kaiware daikon seeds exposed in AMD for 48 hours and rice for 72 hours. (Different letters, a b c, represent statistical differences between treatments; the error bar represents standard deviation; Fisher-LSD multiple comparison; $p < 0.05$ level)

For comparison, a commonly used invasive chemical method for analyzing seed vigor, TTC measurement method was used. TTC is used to differentiate between the metabolically active and inactive seeds. In TTC method, the degree of viability of the seeds can be distinguished by measuring the absorbance of the TPF that is extracted from the ground seeds (Lopez Del Egido et al., 2017)when the white TTC is enzymatically reduced to red TPF (1,3,5 triphenylformazan) due to the activity of various dehydrogenases. The result is shown in Figure 17.

The TPF absorbance of kaiware daikon seeds exposed to 40 ml/L AMD was significantly lower than that of the control, with a 22.0% reduction, and the absorbance of seeds exposed to 80 ml/L AMD was reduced by 54.5% compared to the control. The absorbance of TPF of soybean seeds exposed to 40 ml/L AMD was significantly lower than that of the control with a reduction of by 39.7% while for those exposed to 80ml/L

AMD, the reduction of by 75.7% compared to that of control. These results indicated that the kaiware daikon and soybean seed vigor decreased with increasing AMD concentration. Rice seeds had a different response. The absorbance of TPF of rice seeds in 80ml/L AMD decreased compared to that of the control, but the absorbance of rice seeds in 40ml/L AMD increased by 35.2% compared to that of the control. This result suggested that 40ml/L AMD promoted the rice seed vigor.

The higher the reduction content of TTC, the higher the absorbance and the greater the seed vigor (Zhao et al., 2010) . Kaiware daikon and soybean showed lower seed vigor in 40 ml/L AMD and lowest in 80 ml/L AMD than the control, while rice showed higher seed vigor in 40 ml/L AMD than the control, which showed the same trend as the bOCT results. bOCT results correlated with the internal biological activity of the seeds. TTC can be oxidized in metabolically active seeds. The results suggest that this metabolic activity may be monitored by bOCT.

Iron is an essential micronutrient and sulfur enhances plant tolerance to environmental stresses (Munoz et al., 2009; Nazar et al., 2011). However, excess iron has a negative effect on plants(de Oliveira Jucoski et al., 2013). It is known from the study of Ren et al. concerning the effect of simulated acid rain on rice that rice can survive in a low pH environment but pH lower than 3 had a negative effect on rice (Ren et al., 2018). This evidence supports the result that seed vigor was enhanced at 40 ml/L AMD and inhibited at 80 ml/L AMD.

### 4.2.2 SOD and CAT activity

After one week, all seeds grew into seedlings, except for the soybean seeds in 80 ml/L AMD, which did not germinate. To monitor the response of the antioxidant enzyme system of these seedlings to AMD, we measured the enzyme activities of superoxide dismutase (SOD) and catalase (CAT) (Figure 18). The SOD and CAT activities of kaiware daikon seedlings grown in 40 ml/L AMD were significantly higher compared to the control. And kaiware daikon seedlings grown in 80 ml/L AMD showed significantly lower SOD and

CAT activities compared to the control. Soybean seedlings grown in 40 ml/L AMD had lower SOD and CAT activity, and those grown in 80 ml/L AMD failed to germinate. SOD activity of rice seedlings in 40 ml/L AMD was slightly but not significantly higher compared to the control. While the SOD activity of seedlings in 80 ml/LAMD was significantly lower than that of the control. The CAT activity of rice seedlings in 80 ml/L AMD was significantly lower than that of the control, but there was no significant difference between seedlings in 40 ml/L AMD and the control.

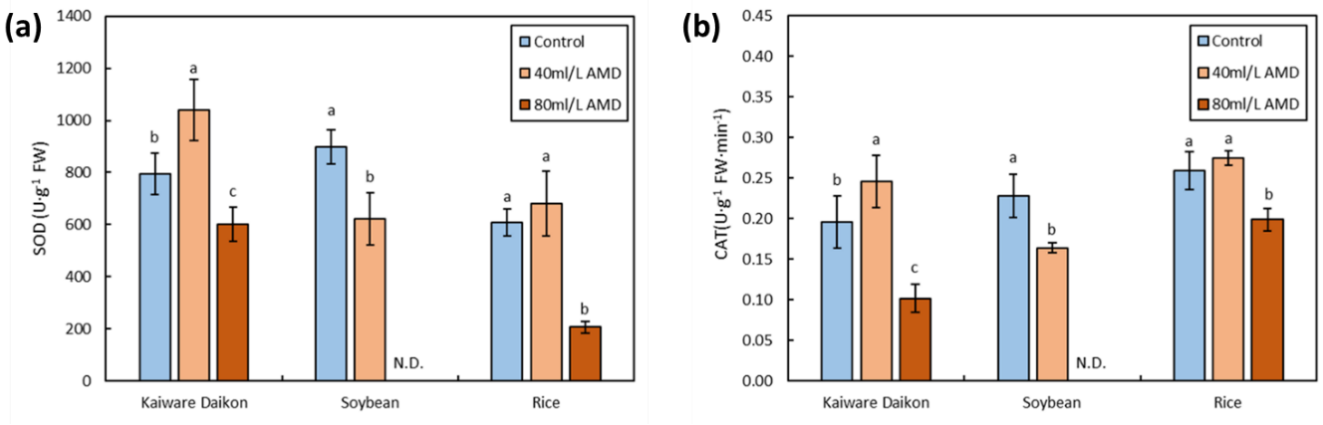


Figure 18 Response of SOD activity and CAT activity of seedlings to AMD after 7 days.

Excessive accumulation of reactive oxygen species (ROS) such as $H_2O_2$ occurs when plants are under environmental stress. SOD is the first defense for scavenging ROS and CAT is the second defense. (Azarabadi et al., 2017). When plants are subjected to environmental stress, the activity of protective enzymes such as SOD and CAT increases to protect the plant. However, when the stress is beyond the plant's tolerance range, the protective enzyme activity decreases (Hasanuzzaman et al., 2012). The results showed that all AMD treatments caused oxidative stress to the kaiware daikon and soybean seedlings, but the rice seedlings grown in 40 ml/L AMD did not receive oxidative stress.

### 4.2.3 $H_2O_2$ and MDA content

To assess the oxidative damage of the seedlings to AMD, we measured the hydrogen peroxide ($H_2O_2$) and malondialdehyde (MDA) content (Table 1). Kaiware daikon seedlings

exposed to 40 ml/L AMD and 80 ml/L AMD showed significantly higher levels of $H_2O_2$ and MDA compared to the control. Soybean seeds exposed to 80 ml/L AMD failed to grow into seedlings, and the $H_2O_2$ and MDA contents in soybean seedlings in 40 ml/L AMD were significantly higher than in the control. The $H_2O_2$ content of rice seedlings in 80 ml/L AMD was significantly higher than that of the control. In contrast, there was no significant difference in the $H_2O_2$ content of rice between the 40 ml/L AMD and control.

When environmental stresses exceed the tolerance range of protective enzymes in plants, excess $H_2O_2$ is accumulated (Caverzan et al., 2012). The results showed that the $H_2O_2$ scavenging system of kaiware daikon and soybean seedling treated with AMD and rice seedlings treated with 80 ml/L AMD was disturbed, while the protective enzymes of rice seedlings in 40 ml/L AMD could function normally. The MDA content of kaiware daikon and soybean seedlings exposed to AMD was significantly elevated. Compared with the control, the MDA content of rice seedlings did not change in 40 ml/L AMD, whereas the MDA content in rice seedlings increased significantly in 80 ml/L AMD. Excessive accumulation of $H_2O_2$ can cause damage to plant cell membranes (Taiz et al., 2015). MDA is one of the important products of membrane lipid peroxidation, so the degree of plant damage can be revealed by measuring MDA content (Stewart and Bewley, 1980). This result indicated that 40 ml/L AMD did not cause damage to rice seedlings. But the membrane of kaiware daikon and soybean seedlings in AMD and rice seedlings in 80 ml/L AMD was severely damaged.

*Table 1* Response of $H_2O_2$ content and MDA content of seedlings to AMD after 7 days.

| Plant species | Treatment | $H_2O_2$ ($\mu mol \cdot g^{-1}$ FW) | MDA ($\mu mol \cdot g^{-1}$ FW) |
|---|---|---|---|
| Kaiware daikon | Control | 1275.49±90.79c | 0.39±0.02b |
| | 40ml/L AMD | 1590.58±66.95b | 0.44±0.04b |
| | 80ml/L AMD | 1942.67±59.25a | 0.87±0.06a |
| Soybean | Control | 794.36±170.27b | 22.21±1.23b |
| | 40ml/L AMD | 1180.36±117.2a | 35.92±3.18a |
| | 80ml/L AMD | N.D. | N.D. |
| Rice | Control | 1453.11±185.43b | 15.15±2.74b |

| | | |
|---|---|---|
| 40ml/L AMD | 1563.43±61.79b | 15.88±1.66b |
| 80ml/L AMD | 1909.39±15.67a | 21.85±2.35a |

Excess iron can induce the production and accumulation of reactive oxygen species (ROS), causing oxidative stress(de Oliveira Jucoski et al., 2013). The pH values of 40 ml/L AMD and 80 ml/L AMD in this study were 2.7 and 3, respectively. A study by Liu et al. demonstrated that antioxidant enzyme activities of soybean seeds increased when the pH was greater than 4, and decreased significantly when the pH was 3.5, 2.5 and 2 (Liu et al., 2011). Wyrwicka et al. demonstrated that the CAT activity of cucumber leaves decreased when the pH was less than 3 (Wyrwicka and Skłodowska, 2006). MDA content of soybeans increased when the pH was less than 4 (Liu et al., 2011).Batty et al. studied the effect of different Fe concentrations on reeds and found that there was an inhibitory effect on reed seedlings when the Fe concentration was greater than 50 mg/L (Batty and Younger, 2003). The content of MDA in rice was significantly increased under the treatment of iron excess(Müller et al., 2015). Rice seedlings grown in simulated acid rain at pH 2.5 showed a substantial increase in MDA content (Ren et al., 2018). In the current study, the antioxidant response of rice seedlings in 40 m/L AMD at pH 3 showed no occurrence of oxidative damage. These studies demonstrate the toxic effects of low pH and high Fe concentrations on plants, which supported the negative effect of 40ml/L AMD and 80ml/L AMD on kaiware daikon and soybean and the negative effect of 80ml/L AMD on rice revealed by bOCT. The critical solution iron concentration at which iron toxicity occurs in rice is highly variable. The reported values range from 10 mg/L to 1000 mg/L Fe, and the variation in the critical solution Fe concentration depends on the growth stage and cultivar of rice(Dobermann, 2000). The iron content in 40 ml/L AMD in this study did not cause iron toxicity to the rice seedlings.

### 4.2.4 Fe concentration

The Fe content concentration from AMD by seedlings was determined after 10 days (Figure 19). In addition to providing insight into the extent to which seedlings are affected by iron in AMD, iron content can be used to speculate whether the inhibitory effect of

AMD is brought about by iron toxicity. The Fe concentration by kaiware daikon seedlings in 40 ml/L AMD was significantly higher than that of the control, and the Fe concentration by kaiware daikon seedlings in 80 ml/L AMD was significantly higher than that of kaiware daikon seedlings in 40 ml/L AMD. There was no significant difference in Fe concentration by soybeans in 40 ml/L AMD and 80 ml/L AMD. The Fe content of rice seedlings in 40 ml/L AMD was significantly higher than that of the control, and the Fe content of rice in 80 ml/L AMD was significantly higher than that of rice in 40 ml/L AMD.

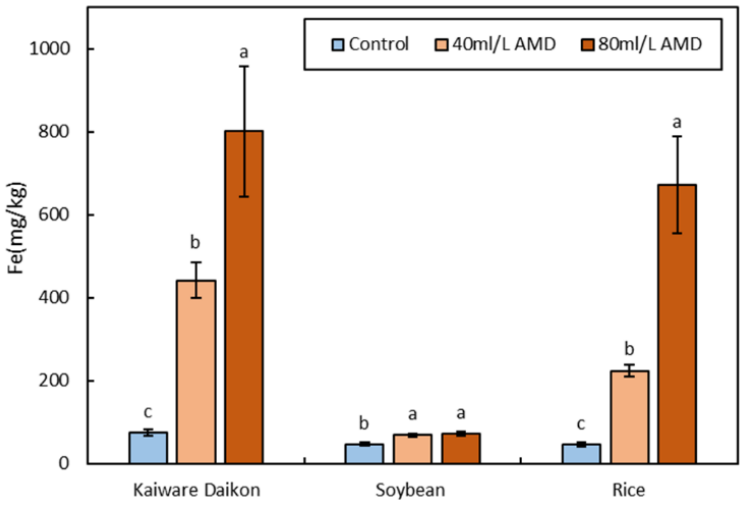


Figure 19 Fe concentration in kaiware daikon, soybean and rice seedlings in AMD after 10 days (different letters, a b c, represent statistical differences between treatments; the error bar represents standard deviation; Fisher-LSD multiple comparison; $p < 0.05$ level).

As mentioned before, Fe is a micronutrient, but in excess it can pose a threat to plants (Morrissey and Guerinot, 2009). The iron concentration of soybean seedlings grown in 40ml/L AMD was higher than that of the control, at 69.29 mg/kg. And the iron concentration of soybeans grown in 80 ml/L AMD was 71.77 mg/kg. There is a risk of damage to plants when Fe accumulation exceed 300 mg/kg (Sahrawat, 2000a) . Soybean seedlings did not accumulate excessive Fe content in each treatment but still showed a negative response, probably due to the inability of soybean to adapt to the low pH environment. Suthipradit et al. showed that soybean seeds grown at pH 3.75 had a 30% reduction in embryonic axis length (Suthipradit and Alva, 1986). Q et al. also indicated that a pH of 3.5 significantly reduced the yield and quality of soybean (Uguru et al., 2012). The pH of the simulated AMD in this study was 2.7 and 3. Therefore, the low pH of AMD

is responsible for the inhibition of shoot and root length in soybean seedlings. Fe accumulation above 300mg/kg can cause damage to rice(Sahrawat, 2000b). Rice seedlings in the 40 ml/L AMD treatment did not exceed the threshold but those in the 80 ml/L AMD far exceeded the threshold. Therefore, seedlings in 80 ml/L AMD showed a negative response. There are no Fe toxicity tests on kaiware daikon, and due to the higher Fe concentration in kaiware daikon grown in AMD, we speculate that one of the reasons for the negative effect of AMD on kaiware daikon is Fe toxicity.

### 4.2.5 Shoot and Root length

The growth and development of plants is an integrated response of various functional and metabolic activities(Alia et al., 2015). Figure 20 shows the photograph of the kaiware daikon' growth under different treatments after 7 days. Depending on AMD treatment levels, the plants growth was significantly different with clear changes in appearance. At the same time, the shoot length and root length of the kaiware daikon seedlings were measured (Figures 20).

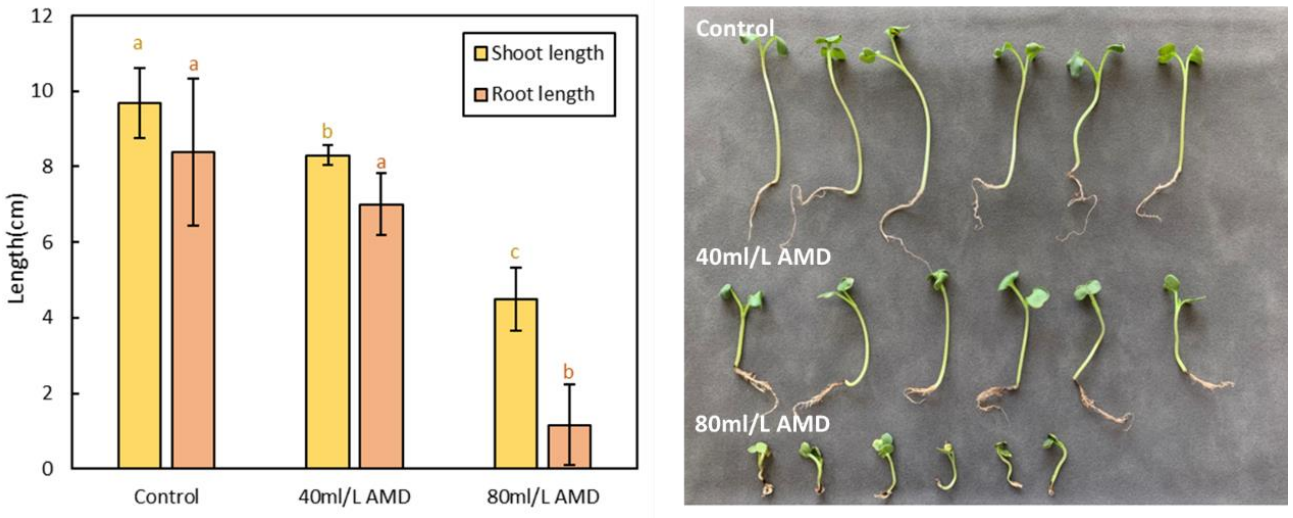


Figure 20 Shoot and root length of Kaiware daikon seedlings after 7 days (Different letters, a b c, represent statistical differences between treatments; the error bar represents standard deviation; Fisher-LSD multiple comparison; $p < 0.05$ level)

There were significant differences in shoot length of the kaiware seedling between treatments (Figure 20). The difference in root length between the control and 80 ml/L AMD treatment was significant but not significant with 40 ml/L AMD treatment. There was a significant difference in the ratio of root to shoot between the control and 80 ml/L AMD treatment, but the difference with 40 ml/L AMD treatment was not significant. These results reveal that AMD inhibits shoot growth, and high concentration AMD inhibits root growth

The tendency of kaiware daikon growth after 7 days was consistent with the bOCT results at 48 h, indicating that the bOCT results could reveal internal activity of the seed much in advance. In addition, there were obvious differences in the morphology of the roots under different treatments (Figure 20). The roots of the plants under 80 mL/L AMD were very short or almost non-existent. The roots of the plants under 40 mL/L AMD had more short branches than the control.

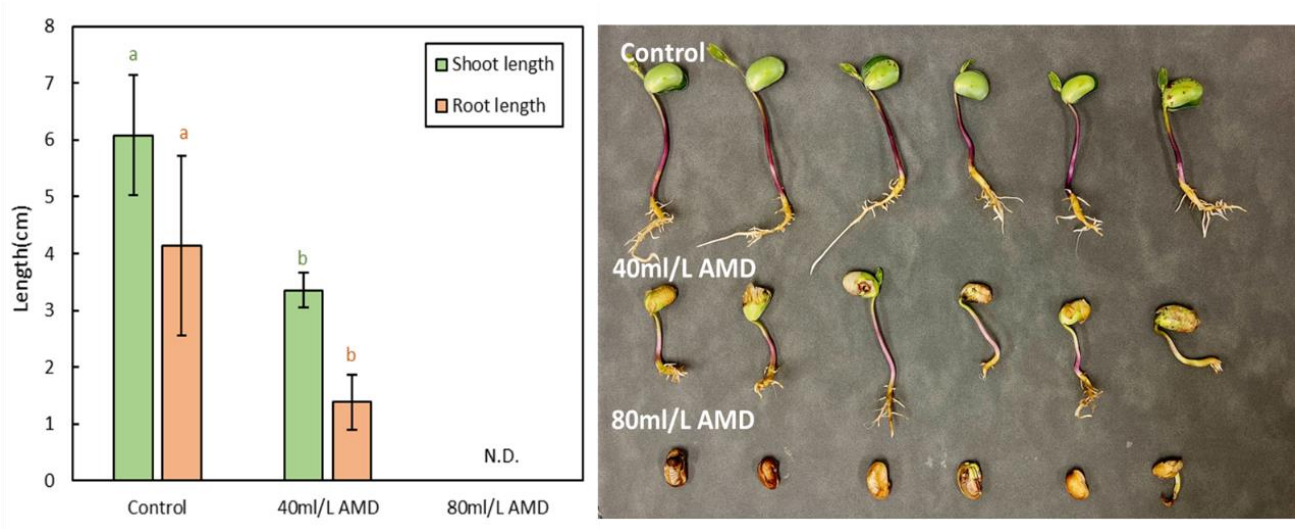


Figure 21 Shoot and root length of soybeanseedlings after 7 days (Different letters, a b c, represent statistical differences between treatments; the error bar represents standard deviation; Fisher-LSD multiple comparison; $p < 0.05$ level)

Soybean seedlings did not accumulate excessive Fe content in each treatment but still showed a negative response, probably due to the inability of soybean to adapt to the low pH environment. Suthipradit et al. showed that soybean seeds grown at pH 3.75 had a 30% reduction in embryonic axis length (Suthipradit and Alva, 1986). Q et al. also indicated that a pH of 3.5 significantly reduced the yield and quality of soybean (Uguru et al., 2012).

The pH of the simulated AMD in this study was 2.7 and 3. Therefore, the low pH of AMD is responsible for the inhibition of shoot and root length in soybean seedlings.

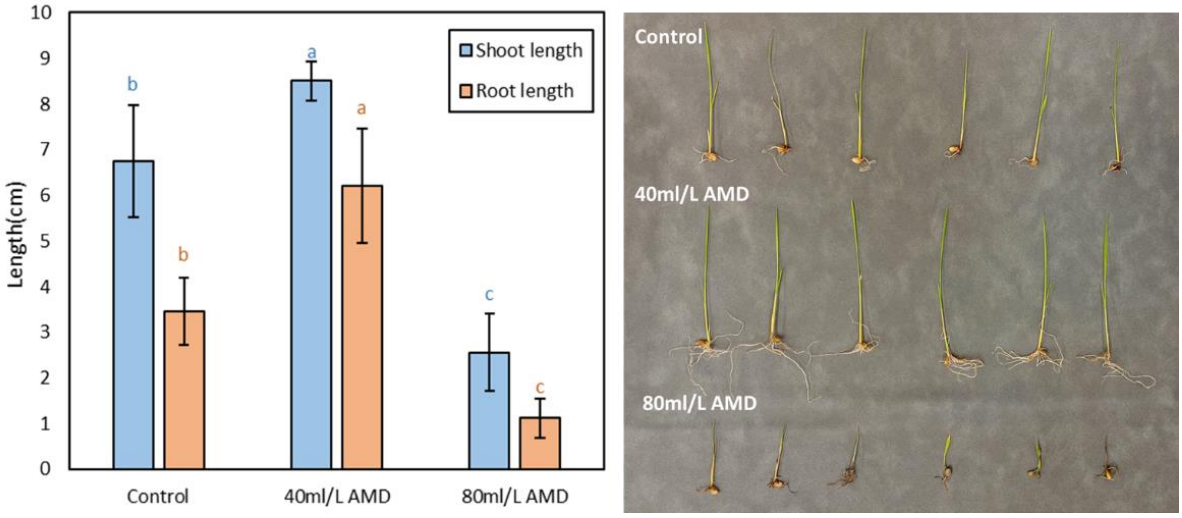


Figure 22 Shoot and root length of rice seedlings after 10 days (Different letters, a b c, represent statistical differences between treatments; the error bar represents standard deviation; Fisher-LSD multiple comparison; $p < 0.05$ level)

After 10 days, the growth status of rice seedlings under different concentrations of AMD treatment began to show differences. Then shoot and root length were measured (Figure 22). The shoot and root lengths of rice grown in different concentrations of AMD were significantly different after 10 days. Seedlings grown in 40 ml/L AMD had significantly higher shoot and root lengths than that of the control. While the roots of rice in 80 ml/L AMD could hardly grow normally. The results showed that high concentrations of AMD significantly inhibited the rice growth, while low concentrations of AMD could even promote the seedling growth. The reasons for this result may be that the iron ions in low concentrations of AMD can serve as a nutrient element for rice(Alia et al., 2015). Iron is essential for chlorophyll synthesis, and in addition, the root system is dependent on iron for proper development (Ghafariyan et al., 2013; Römheld and Marschner, 1981). But excessive iron brings iron toxicity to plants(Morrissey and Guerinot, 2009) which supports our results that both roots and shoots of rice seedlings were significantly promoted in 40 ml/L AMD while inhibited in 80 ml/L AMD.

## 4.3 Conclusion

Combined with the results of 1-hour bOCT and the percentage of germination within 48 hours, it was found that bOCT could observe the change of kaiware daikon seed internal activity after only 1 hour when the seeds were under AMD stress. The lower average biospeckle contrast of kaiware daikon and soybean seeds obtained by the bOCT method revealed the lower biological activity of kaiware daikon and soybean seeds in 40ml/L and 80 ml/L AMD after 48 hours. At the same time, the TTC results revealed that kaiware daikon and soybean seed vigor was higher in control and lower in 40ml/L and 80 ml/L AMD. The results from the antioxidant system after one week showed that kaiware daikon and soybean seedlings were were stressed in 40 ml/L AMD and 80 ml/L AMD. The iron concentration results showed that the kaiware daikon and soybean seedlings in 40 ml/L AMD and 80 ml/L AMD were exposed to iron toxicity The shoot and root length of kaiware daikon and soybean seedlings after 7 days showed the the inhibiting effect of 40 ml/L AMD and 80 ml/L AMD.

The higher average biospeckle contrast obtained by the bOCT method revealed the higher biological activity of rice seeds after 72 hours exposure to 40 ml/L AMD and the lower average biospeckle contrast obtained revealed the lower biological activity of rice seeds in 80 ml/L AMD. At the same time, the TTC results revealed that rice seed vigor was increased in 40 ml/L AMD and decreased in 80 ml/L AMD. The results from the antioxidant system after one week showed that rice seedlings were not stressed in 40 ml/L AMD but were stressed in 80 ml/L AMD. The iron concentration results showed that the rice seedlings in 80 ml/L AMD were exposed to iron toxicity while the rice seedlings in 40 ml/L AMD were not. The shoot and root length of rice seedlings after ten days showed the promoting effect of 40 ml/L AMD and the inhibiting effect of 80 ml/L AMD.

# Chapter 5 Monitoring plant growth behavior under AMD exposure by SIT

## 5.1 SIT Results and Discussion

In bOCT experiments we found that rice seeds responded differently from Kaiware daikon and soybean at 40 ml/L AMD, and the same tendency was obtained by traditional indicators such as seed vigor, enzyme activity, and shoot length and root length of seedlings. The specific response of rice in AMD was of interest to us, therefore we monitored rice seedlings by SIT method.

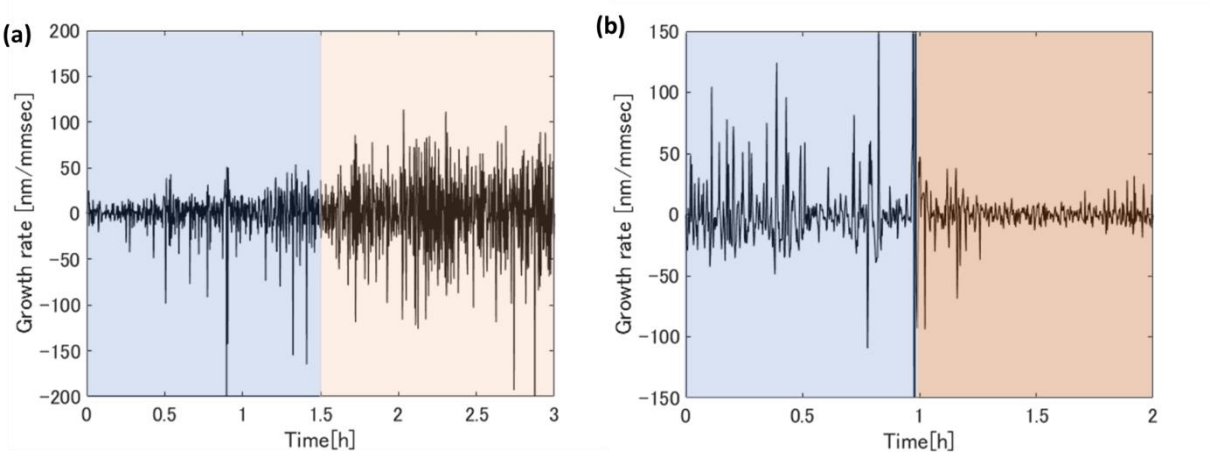


Figure 23 NIF of rice leaf shown as a function of the measurement period under (a) control condition change to 40ml/L AMD, and (b) control condition change to 80ml/L AMD. Note the fluctuations are in the order of nanometer indicating the sensitivity of SIT.

As shown in the Figure 23, SIT monitored different nanometric intrinsic fluctuations (NIF) of rice leaves in distilled water and in simulated AMD. The NIF of rice leaves was promoted when the root environment was changed from distilled water to 40 ml/L AMD; The NIF of rice leaves was inhibited when the root environment was changed from distilled water to 80 ml/L AMD.

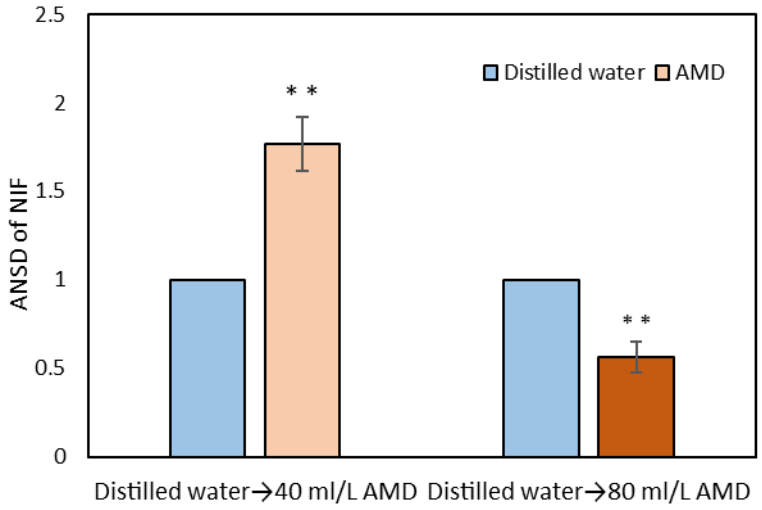


Figure 24 ANSD (average normalized standard deviation) of NIF of rice leaf exposed to distilled water as control and different concentration of AMD. (* * indicates significant difference at $p<0.01$.)

Standard deviations (SD) of NIF were calculated to evaluate the dependence of NIF on the environmental conditions. Normalization was done to exclude the individual variaton among the samples during a single session. The average normalized standard deviation (ANSD) of NIF of rice leaf was shown in Figure 24. The results showed a significant difference in the NIF under AMD compared to the control. The ANSD of rice leaves increased significantly by 76.7% when rice roots were transferred from distilled water to 40 ml/L AMD, and decreased significantly by 43.7% when rice roots were transferred from distilled water to 80 ml/L AMD.

The reason for the presence of nanoscale fluctuations is unclear. DeSilva et al. hypothesized that these fluctuations may be related to intrinsic plant properties independent of any external factors, thus reflecting microscopic processes that are clearly related to the physiological state of the plant (DeSilva et al., 2017). A proper balance is maintained between cellular compression and cell wall extensibility during plant growth. An organ's cells share a common cell wall and water, so oscillation is a reasonable way to synchronize cell growth. Due to the fact that cell expansion is a complex cellular process involving a number of steps, the cell wall is insufficient to synchronize the growth of a thousand adjacent cells: the concentration of water, secretion, incorporation of material, and

irreversible, i.e., plastic, and reversible, i.e., elastic deformation of the cell wall structure. There may be feedback associated with all of these processes, resulting in oscillations (Mancuso and Shabala, 2015). The results of this experiment showed that the NIF of rice leaves was promoted in 40 ml/L AMD and inhibited in 80 ml/L AMD, probably because the pH of 40 ml/L AMD could soften the cell wall and the appropriate concentration of Fe could promote the growth of rice seedlings but the pH of 80 ml/L AMD was too low and the concentration of Fe was high, which was harmful to the rice growth.

## 5.2 Conclusion

Statistical interferometric technique (SIT) is a highly sensitive, high speed and non-invasive optical technique developed by our group capable of measuring instantaneous sub-nanometer displacements. SIT applied to plant leaf elongation revealed nanometric intrinsic fluctuations (NIF) that are reliable and sensitive to variations in the environment making NIF as a measure of healthiness of the plants. In this study, we applied SIT to monitor the characteristic of NIF of rice seedlings under simulated acid mine drainage (AMD). NIF showed significant reductions under 80ml/L AMD indicating the negative effect on rice growth dynamics. In contrast, significant increments of NIF could be observed under 40ml/L AMD conditions indicating the positive effect on rice growth. Such effects were also revealed by biospeckle optical coherence tomography in chapter 4. The results of shoot and root length (Figure 22) could also support the SIT results. SIT permitted a reliable, sensitive, and accurate measurement that could become possibly new indicator on the plant growth at sub-nanometer accuracy.

# Chapter 6 Conclusion

The biospeckle contrast of seeds measured by the proposed bOCT method was significantly lower in Kaiware daikon and soybean seeds after 48 hours exposure to simulated AMD compared to the control; the response of rice differed from Kaiware daikon and soybean, and the biospeckle contrast of rice seeds after 72 hours exposure to 40 ml/L AMD was significantly higher than that of the control. We hypothesized that the difference in biospeckle contrast is due to the biological activity within the seeds and is related to the health of the seeds. Thus, to prove the hypothesis, some of the conventional indicators commonly used to determine the plant physiology were measured, including seed vigor, seedling enzyme activity, iron concentration, shoot length and root length. Eventually, a consistent tendency was found between the results of the conventional methods and those measured by the bOCT method. Since our proposed bOCT method has the advantages of non-invasive and very short measurement time, it does not destroy the seeds and allows multiple monitoring of the same sample. In addition, the efficient and rapid determination makes it possible to determine many samples in a short time and can be used as a rapid screening method for plant varieties. Further, the high sensitivity of the SIT method to environmental changes was verified by SIT monitoring the NIF changes of rice leaves under simulated AMD. In this study, we applied SIT, focusing on the effects of AMD on rice seedlings, and demonstrated that it can be an effective method to monitor plant responses to AMD

.

# References


Aizu, Y.a., Asakura, T., 1991. Bio-speckle phenomena and their application to the evaluation of blood flow. Optics & Laser Technology 23, 205-219.

Akcil, A., Koldas, S., 2006. Acid Mine Drainage (AMD): causes, treatment and case studies. Journal of cleaner production 14, 1139-1145.

Alia, F.J., Shamshuddin, J., Fauziah, C.I., Husni, M.H.A., Panhwar, Q.A., 2015. Effects of Aluminum, Iron and/or Low pH on Rice Seedlings Grown in Solution Culture. International Journal of agriculture and Biology 17.

Alves, J.A., Júnior, R.A.B., Boas, E.V.d.B.V., 2013. Identification of respiration rate and water activity change in fresh-cut carrots using biospeckle laser and frequency approach. Postharvest Biology and Technology 86, 381-386.

Anna, T., Chakraborty, S., Cheng, C.-Y., Srivastava, V., Chiou, A., Kuo, W.-C., 2019. Elucidation of microstructural changes in leaves during senescence using spectral domain optical coherence tomography. Scientific reports 9, 1-10.

Azarabadi, S., Abdollahi, H., Torabi, M., Salehi, Z., Nasiri, J., 2017. ROS generation, oxidative burst and dynamic expression profiles of ROS-scavenging enzymes of superoxide dismutase (SOD), catalase (CAT) and ascorbate peroxidase (APX) in response to Erwinia amylovora in pear (Pyrus communis L). European Journal of Plant Pathology 147, 279-294.

Batty, L.C., Younger, P.L., 2003. Effects of external iron concentration upon seedling growth and concentration of Fe and phosphate by the common reed, Phragmites australis (Cav.) Trin ex. Steudel. Annals of Botany 92, 801-806.

Briers, J.D., 2001. Time-varying laser speckle for measuring motion and flow, Saratov Fall Meeting 2000: Coherent Optics of Ordered and Random Media. SPIE, pp. 25-39.

Caverzan, A., Passaia, G., Rosa, S.B., Ribeiro, C.W., Lazzarotto, F., Margis-Pinheiro, M., 2012. Plant responses to stresses: Role of ascorbate peroxidase in the antioxidant protection. Genet Mol Biol 35, 1011-1019.

Chamorro, S., Barata, C., Piña, B., Casado, M., Schwarz, A., Sáez, K., Vidal, G., 2018. Toxicological analysis of acid mine drainage by water quality and land use bioassays. Mine Water and the Environment 37, 88-97.

Dainty, J., 1984. Laser speckle and related phenomena. Topics in Applied Physics 9, 203-253.

de Oliveira Jucoski, G., Cambraia, J., Ribeiro, C., de Oliveira, J.A., de Paula, S.O., Oliva, M.A., 2013. Impact of iron toxicity on oxidative metabolism in young Eugenia uniflora L. plants. Acta physiologiae plantarum 35, 1645-1657.

De Silva, Y., Rajagopalan, U., Kadono, H., 2021a. Microplastics on the growth of plants and seed germination in aquatic and terrestrial ecosystems. Global Journal of Environmental Science and Management.

De Silva, Y.S.K., Rajagopalan, U.M., Kadono, H., Li, D., 2021b. Positive and negative phenotyping of increasing Zn concentrations by Biospeckle Optical Coherence Tomography in speedy monitoring on lentil (Lens culinaris) seed germination and seedling growth. Plant Stress 2, 100041.

De Silva, Y.S.K., Rajagopalan, U.M., Li, D., Kadono, H., 2022. Optical screening method to observe the biological activities of lentil (Lens culinaris) seeds quantitatively under the exposure of polyethylene microplastics (PEMPs) using ultrahigh accurate biospeckle optical coherence tomography, Tissue Optics and Photonics II. SPIE, pp. 70-77.

de Wit, J., Tonn, S., Van den Ackerveken, G., Kalkman, J., 2020. Quantification of plant morphology and leaf thickness with optical coherence tomography. Applied Optics 59, 10304-10311.
DeSilva, K.T.K.M., Rajagopalan, U.M., Kadono, H., 2017. Highly sensitive optical interferometric technique reveals stress-dependent instantaneous nanometric growth fluctuations of Chinese chive leaf under heavy metal stress. Ecotoxicology and environmental safety 137, 86-93.
Dobermann, A., 2000. Rice: Nutrient disorders & nutrient management. Int. Rice Res. Inst.
Dong, Y., Liu, F., Qiao, X., Zhou, L., Bi, W., 2018. Effects of acid mine drainage on calcareous soil characteristics and Lolium perenne L. germination. International Journal of Environmental Research and Public Health 15, 2742.
Draijer, M., Hondebrink, E., van Leeuwen, T., Steenbergen, W., 2009. Review of laser speckle contrast techniques for visualizing tissue perfusion. Lasers in medical science 24, 639-651.
Gajewska, E., Skłodowska, M., 2008. Differential biochemical responses of wheat shoots and roots to nickel stress: antioxidative reactions and proline accumulation. Plant Growth Regulation 54, 179-188.
Garrido, A., Condori, J., Strosnider, W., Nairn, R., 2009. Acid mine drainage impacts on irrigation water resources, agricultural soils, and potatoes in Potosi, Bolivia. Proceedings America Society of Mining and Reclamation, 486-499.
Ghafariyan, M.H., Malakouti, M.J., Dadpour, M.R., Stroeve, P., Mahmoudi, M., 2013. Effects of magnetite nanoparticles on soybean chlorophyll. Environ Sci Technol 47, 10645-10652.
Hariharan, P., 2003. Interference microscopy. Academic Press, Elsevier Amsterdam, the Netherlands.
Hasanuzzaman, M., Hossain, M.A., Silva, J.A., Fujita, M., 2012. Plant response and tolerance to abiotic oxidative stress: antioxidant defense is a key factor, Crop stress and its management: perspectives and strategies. Springer, pp 261-315.
Houston, K., Tucker, M.R., Chowdhury, J., Shirley, N., Little, A., 2016. The plant cell wall: a complex and dynamic structure as revealed by the responses of genes under stress conditions. Frontiers in plant science 7, 984.
Huang, X., Li, N., Wu, Q., Long, J., Luo, D., Zhang, P., Yao, Y., Huang, X., Li, D., Lu, Y., 2016. Risk assessment and vertical distribution of thallium in paddy soils and concentration in rice plants irrigated with acid mine drainage. Environmental Science and Pollution Research 23, 24912-24921.
Hughes, A., Cockshull, K., Heath, O., 1970. Leaf area and absolute leaf water content. Annals of Botany 34, 259-266.
Islam, A., Edwards, D., Asher, C., 1980. pH optima for crop growth. Plant and soil 54, 339-357.
Joshi, D., Butola, A., Kanade, S.R., Prasad, D.K., Mithra, S.A., Singh, N., Bisht, D.S., Mehta, D.S., 2021. Label-free non-invasive classification of rice seeds using optical coherence tomography assisted with deep neural network. Optics & Laser Technology 137, 106861.
Khan, R.A., Khan, A., Qadri, T.A., 2019. Influence of seed priming with FeSO4 on germination, growth and biochemical aspects of mung bean (Vigna radiata L.) grown under NaCl stress. Journal of Bioscience and Applied Research 5, 519-532.
Kiiskila, J.D., Li, K., Sarkar, D., Datta, R., 2020. Metabolic response of vetiver grass (Chrysopogon zizanioides) to acid mine drainage. Chemosphere 240, 124961.
Larimer, C.J., Denis, E.H., Suter, J.D., Moran, J.J., 2020. Optical coherence tomography imaging of plant root growth in soil. Applied Optics 59, 2474-2481.
Li, D., Rajagopalan, U.M., De Silva, Y.S.K., Liu, F., Kadono, H., 2021. Biospeckle optical coherence tomography (BOCT) in the speedy assessment of the responses of the seeds of Raphanus sativus L.(Kaiware Daikon) to acid mine drainage (AMD). Applied Sciences 12, 355.

Liao, J., Wen, Z., Ru, X., Chen, J., Wu, H., Wei, C., 2016. Distribution and migration of heavy metals in soil and crops affected by acid mine drainage: Public health implications in Guangdong Province, China. Ecotoxicology and environmental safety 124, 460-469.
Lim, Y., Funada, K., Kadono, H., 2019. Monitor biological activities in seed germination by biospeckle optical coherence tomography, Dynamics and Fluctuations in Biomedical Photonics XVI. SPIE, pp. 42-47.
Lim, Y., Kadono, H., 2020. Evaluation of germination ability of seeds at different temperatures by biospeckle optical coherence tomography, Tissue Optics and Photonics. SPIE, pp. 27-32.
Liu, T.T., Wu, P., Wang, L.H., Zhou, Q., 2011. Response of soybean seed germination to cadmium and acid rain. Biological Trace Element Research 144, 1186-1196.
Lopez Del Egido, L., Navarro-Miró, D., Martinez-Heredia, V., Toorop, P.E., Iannetta, P.P., 2017. A spectrophotometric assay for robust viability testing of seed batches using 2, 3, 5-triphenyl tetrazolium chloride: using Hordeum vulgare L. as a model. Frontiers in plant science 8, 747.
Mancuso, S., Shabala, S., 2015. Rhythms in plants: dynamic responses in a dynamic environment. Springer.
Mangabeira, P.A., Ferreira, A.S., de Almeida, A.-A.F., Fernandes, V.F., Lucena, E., Souza, V.L., dos Santos Júnior, A.J., Oliveira, A.H., Grenier-Loustalot, M.F., Barbier, F., 2011. Compartmentalization and ultrastructural alterations induced by chromium in aquatic macrophytes. Biometals 24, 1017-1026.
Manhando, E., Zhou, Y., Wang, F., 2021. Early Detection of Mold-Contaminated Peanuts Using Machine Learning and Deep Features Based on Optical Coherence Tomography. AgriEngineering 3, 703-715.
Mapanda, F., Nyamadzawo, G., Nyamangara, J., Wuta, M., 2007. Effects of discharging acid-mine drainage into evaporation ponds lined with clay on chemical quality of the surrounding soil and water. Physics and Chemistry of the Earth, Parts A/B/C 32, 1366-1375.
Marcos, J., 2015. Seed vigor testing: an overview of the past, present and future perspective. Scientia Agricola 72, 363-374.
Matlock, M.M., Howerton, B.S., Atwood, D.A., 2002. Chemical precipitation of heavy metals from acid mine drainage. Water research 36, 4757-4764.
Mittler, R., 2002. Oxidative stress, antioxidants and stress tolerance. Trends in plant science 7, 405-410.
Moatter, K., Khan, A.M., Iqbal, S., Dilshad, I., Qadri, T.A., Abdullah, F., Gilani, S.A., 2020. 17. Effects of seed priming with PbSO4 and FeSO4 on germination and growth of seedlings of Beta vulgaris L. under NaCl stress. Pure and Applied Biology (PAB) 9, 1405-1423.
Morrissey, J., Guerinot, M.L., 2009. Iron concentration and transport in plants: the good, the bad, and the ionome. Chem Rev 109, 4553-4567.
Müller, C., Kuki, K.N., Pinheiro, D.T., de Souza, L.R., Siqueira Silva, A.I., Loureiro, M.E., Oliva, M.A., Almeida, A.M., 2015. Differential physiological responses in rice upon exposure to excess distinct iron forms. Plant and Soil 391, 123-138.
Munoz, M., Villar, I., Garcia-Erce, J.A., 2009. An update on iron physiology. World J Gastroenterol 15, 4617-4626.
Murata, M., Hammes, P., Zharare, G., 2003. Effect of solution pH and calcium concentration on germination and early growth of groundnut. Journal of Plant Nutrition 26, 1247-1262.
Nazar, R., Iqbal, N., Masood, A., Syeed, S., Khan, N.A., 2011. Understanding the significance of sulfur in improving salinity tolerance in plants. Environmental and Experimental Botany 70, 80-87.

Nemeth, A., Hannesschläger, G., Leiss-Holzinger, E., Wiesauer, K., Leitner, M., 2013. Optical coherence tomography–applications in non-destructive testing and evaluation. Optical coherence tomography 6, 163-186.
Organization, W.H., 2020. The state of food security and nutrition in the world 2020: transforming food systems for affordable healthy diets. Food & Agriculture Org.
Perico, C., Sparkes, I., 2018. Plant organelle dynamics: cytoskeletal control and membrane contact sites. New Phytologist 220, 381-394.
Prasad, B., Maity, S., Mondal, M.R., Singh, K.K.K., 2021. Evaluation of Treatment Techniques for Utilising Acid Mine Water in Agriculture. Water, Air, & Soil Pollution 232, 1-17.
Rajagopalan, U.M., Kabir, M., Lim, Y., Kadono, H., 2020. Biospeckle optical coherence tomography in speedy visualizing effects of foliar application of plant growth hormone to Chinese chives leaves. BMC research notes 13, 1-6.
Ramírez-Miquet, E.E., Cabrera, H., Grassi, H.C., Andrades, E.d.J., Otero, I., Rodríguez, D., Darias, J.G., 2017. Digital imaging information technology for biospeckle activity assessment relative to bacteria and parasites. Lasers in medical science 32, 1375-1386.
Rateria, A., Mohan, M., Mukhopadhyay, K., Poddar, R., 2019. Investigation of Puccinia triticina contagion on wheat leaves using swept source optical coherence tomography. Optik 178, 932-937.
Ren, X.Q., Zhu, J.Z., Liu, H.Y., Xu, X., Liang, C.J., 2018. Response of antioxidative system in rice (Oryza sativa) leaves to simulated acid rain stress. Ecotoxicology and Environmental Safety 148, 851-856.
Römheld, V., Marschner, H., 1981. Iron deficiency stress induced morphological and physiological changes in root tips of sunflower. Physiologia Plantarum 53, 354-360.
Sahrawat, K.á., 2000a. Elemental composition of the rice plant as affected by iron toxicity under field conditions. Communications in soil science and plant analysis 31, 2819-2827.
Sahrawat, K.L., 2000b. Elemental composition of the rice plant as affected by iron toxicity under field conditions. Communications in Soil Science and Plant Analysis 31, 2819-2827.
Sies, H., 2014. Role of metabolic H2O2 generation: redox signaling and oxidative stress. Journal of Biological Chemistry 289, 8735-8741.
Simate, G.S., Ndlovu, S., 2014. Acid mine drainage: Challenges and opportunities. Journal of Environmental Chemical Engineering 2, 1785-1803.
Srimal, L., Kadono, H., Rajagopalan, U., 2013. Optical coherence tomography biospeckle imaging for fast monitoring varying surface responses of a plant leaf under ozone stress, Sensing Technologies for Biomaterial, Food, and Agriculture 2013. International Society for Optics and Photonics, p. 88810H.
Srimal, L., Rajagopalan, U., Kadono, H., 2015. Functional optical coherence tomography (fOCT) biospeckle imaging to investigate response of plant leaves to ultra-short term exposure of Ozone, Journal of Physics: Conference Series. IOP Publishing, p. 012013.
Srivastava, R., Chen, Y., Deng, Y., Brandizzi, F., Howell, S.H., 2012. Elements proximal to and within the transmembrane domain mediate the organelle-to-organelle movement of bZIP28 under ER stress conditions. The Plant Journal 70, 1033-1042.
Stewart, R.R., Bewley, J.D., 1980. Lipid peroxidation associated with accelerated aging of soybean axes. Plant Physiol 65, 245-248.
Suthipradit, S., Alva, A., 1986. Aluminum and pH limitations for germination and radicle growth of soybean. Journal of plant nutrition 9, 67-73.
Szymanska-Chargot, M., Adamiak, A., Zdunek, A., 2012. Pre-harvest monitoring of apple fruits development with the use of biospeckle method. Scientia Horticulturae 145, 23-28.
Taiz, L., Zeiger, E., 2002. Plant physiology, 3rd edn. Sunderland, MA. Sinauer Associates, Inc.

Taiz, L., Zeiger, E., Møller, I.M., Murphy, A., 2015. Plant physiology and development. Sinauer Associates Incorporated.
Uguru, M.I., Oyiga, B.C., Jandong, E.A., 2012. Responses of some soybean genotypes to different soil pH regimes in two planting seasons. The African Journal of Plant Science and Biotechnology 6, 26-37.
Wada, M., Suetsugu, N., 2004. Plant organelle positioning. Current opinion in plant biology 7, 626-631.
Wang, H., Zeng, Y., Guo, C., Bao, Y., Lu, G., Reinfelder, J.R., Dang, Z., 2018. Bacterial, archaeal, and fungal community responses to acid mine drainage-laden pollution in a rice paddy soil ecosystem. Science of the Total Environment 616, 107-116.
Wang, X., Sheng, X., Tian, X., Zhang, Y., Li, Y., 2020a. Organelle movement and apical accumulation of secretory vesicles in pollen tubes of Arabidopsis thaliana depend on class XI myosins. Plant J 104, 1685-1697.
Wang, X., Sheng, X., Tian, X., Zhang, Y., Li, Y., 2020b. Organelle movement and apical accumulation of secretory vesicles in pollen tubes of Arabidopsis thaliana depend on class XI myosins. The Plant Journal 104, 1685-1697.
Wijesinghe, R.E., Lee, S.-Y., Ravichandran, N.K., Shirazi, M.F., Kim, P., Jung, H.-Y., Jeon, M., Kim, J., 2018. Biophotonic approach for the characterization of initial bitter-rot progression on apple specimens using optical coherence tomography assessments. Scientific Reports 8, 1-10.
Williamson, R.E., 1993. Organelle Movements. Annual Review of Plant Physiology and Plant Molecular Biology 44, 181-202.
Wyrwicka, A., Skłodowska, M., 2006. Influence of repeated acid rain treatment on antioxidative enzyme activities and on lipid peroxidation in cucumber leaves. Environmental and Experimental Botany 56, 198-204.
Yang, Q., Tang, L., Shen, M., Wang, Y., Wei, Y., Jeyalatha, V., Chen, P., Dong, F., Wang, G., Wu, S., 2018. Effects of diesel exhaust particles on the condition of mouse ocular surface. Ecotoxicology and Environmental Safety 163, 585-593.
Zdunek, A., Adamiak, A., Pieczywek, P.M., Kurenda, A., 2014. The biospeckle method for the investigation of agricultural crops: A review. Optics and Lasers in Engineering 52, 276-285.
Zhao, P.F., Zhu, Y.H., Wang, W., 2010. Evaluation and improvement of spectrophotometric assays of TTC reduction: maize (Zea mays) embryo as an example. Acta Physiologiae Plantarum 32, 815-819.

# Appendix

*Table A1 Initial metal concentrations from the Pikeville AMD site*

| Element | Borehole conc. (ppm) | 3″ pipe conc. (ppm) | 4″ pipe conc. (ppm) | Discharge conc. (ppm) | Downstream conc. (ppm) |
|---|---|---|---|---|---|
| Al | 0.483 | 0.515 | 0.452 | 0.641 | 0.567 |
| Sb | 1.31 | 0.394 | 0.339 | 0.249 | 0.210 |
| As | 0.017 | <0.012 | <0.012 | <0.012 | <0.012 |
| Ba | 0.007 | 0.015 | 0.019 | 0.012 | 0.018 |
| Be | 0.001 | 0.001 | <0.001 | <0.001 | <0.001 |
| Cd | 0.010 | <0.008 | <0.008 | <0.008 | <0.008 |
| Cr | <0.014 | <0.014 | <0.014 | <0.014 | <0.014 |
| Co | 0.023 | 0.011 | 0.010 | 0.008 | 0.007 |
| Cu | 0.012 | <0.009 | <0.009 | <0.009 | <0.009 |
| Fe | 194 | 28.4 | 24.2 | 2.88 | 2.70 |
| Pb | <0.020 | <0.020 | <0.020 | <0.020 | <0.020 |
| Mg | 57.4 | 57.1 | 49.4 | 52.6 | 42.9 |
| Mn | 4.65 | 2.65 | 2.18 | 1.25 | 0.913 |
| Se | 0.022 | 0.022 | 0.029 | <0.011 | <0.011 |
| Sr | 3.53 | 5.68 | 4.92 | 5.10 | 4.29 |